

Lattice vibrations of α' - NaV_2O_5 in the low-temperature phase. Magnetic bound states?

M. N. Popova, A. B. Sushkov, S. A. Klimin, E. P. Chukalina
*Institute of Spectroscopy of Russian Academy of Sciences,
142190 Troitsk, Moscow reg., Russia*

B. Z. Malkin
Kazan State University, 420008 Kazan, Russia

M. Isobe, Yu. Ueda
*Institute for Solid State Physics, The University of Tokyo
7-22-1 Roppongi, Minato-ku, Tokyo 106, Japan
(October 31, 2018)*

We report high resolution polarized infrared studies of the quarter-filled spin ladder compound α' - NaV_2O_5 as a function of temperature ($5 \text{ K} \leq T \leq 300 \text{ K}$). Numerous new modes were detected below the temperature $T_c = 34 \text{ K}$ of the phase transition into a charge ordered nonmagnetic state accompanied by a lattice dimerization. We analyse the Brillouin zone (BZ) folding due to lattice dimerization at T_c and show that some peculiarities of the low-temperature vibrational spectrum come from quadruplets folded from the BZ point $(\frac{1}{2}, \frac{1}{2}, \frac{1}{4})$. We discuss an earlier interpretation of the 70, 107, and 133 cm^{-1} modes as magnetic bound states and propose the alternative interpretation as folded phonon modes strongly interacting with charge and spin excitations.

PACS numbers: 78.30.-j, 63.20.-e, 63.20.Ls

I. INTRODUCTION

The magnetic insulator α' - NaV_2O_5 has received a considerable attention since 1996, when Isobe and Ueda reported a spin-Peierls-like transition at $T_c = 35 \text{ K}$ [1]. The structure of this vanadate consists of two-leg ladders formed by corner-sharing distorted V_2O_5 pyramids running along the orthorhombic b -axis, with their rungs along the a -axis (see Fig. 1). Neighboring ladders are linked via common edges of the pyramids to form the ab -layers. Na atoms lie between the layers. At room temperature, the structure is centrosymmetric (space group $Pm\bar{m}n-D_{2h}^{13}$) with only one crystallographic position for vanadium having a formal valence $+4.5$ [2–7]. As a result, one electron is shared by two V atoms and is actually distributed over a V–O–V molecular orbital at the ladder rung. A quarter-filled ladder along the b -direction is formed, which explains one-dimensional magnetic properties of α' - NaV_2O_5 above T_c [2,8].

Below T_c , a steep isotropic decrease of the magnetic susceptibility corresponding to a singlet-triplet gap of $\Delta=85 \text{ K}$ [1,9] and a lattice dimerization described by the propagation wave vector $\mathbf{k} = (\frac{1}{2}, \frac{1}{2}, \frac{1}{4})$ [10] were recently found to be accompanied by a charge ordering of a zigzag type [7,11–13]. The nature of the state below T_c is presently under intense investigation. The recent synchrotron X-ray diffraction studies of the low-temperature (LT) structure [6,14,15] resulted in the acentric space group $Fmm2-C_{2v}^{18}$ with three essentially different positions for the vanadium atoms arranged into a sequence of zigzag modulated ladders separated by nonmodulated ones (see Fig. 1). The corresponding three vanadium valence states, $+4$, $+5$, and $+4.5$, have been suggested from the bond-valence analysis in Ref. [16]. This finding contradicts the NMR observation of only two inequivalent electronic states of vanadium below T_c [7]. More recent bond-valence calculations suggest, however, only two vanadium valences despite the three crystallographically inequivalent V sites [15]. Nevertheless, several observations, in particular, the properties of X-ray anomalous scattering [13], can be better explained if one assumes the modulation of all the vanadium ladders, and therefore different subgroups of $Fmm2$ were considered [17,18]. In their Raman scattering study of folded modes, the authors of Ref. [19] claimed the centrosymmetric $C2/c$ group for the LT-phase of α' - NaV_2O_5 , from purely spectroscopic reasons.

Folded modes of the dimerized lattice of α' - NaV_2O_5 have been observed first in the far infrared (FIR) transmission [20], then Raman scattering [9,21,22] and FIR reflection [23,24] measurements. Only two out of more than thirty observed [20,25,23,24] new low-temperature FIR modes, namely, the modes at 718 cm^{-1} ($\mathbf{E} \parallel \mathbf{a}, \mathbf{b}$) [23,26,24] and 960 cm^{-1} ($\mathbf{E} \parallel \mathbf{a}$) [24] have been studied in detail. Three lowest frequency Raman lines ($67, 107, 133 \text{ cm}^{-1}$) that emerge below T_c have been attributed to magnetic singlet bound states [22,27,28]. The recent work [29] called this interpretation into question, however. Thus, both the low-temperature structure of α' - NaV_2O_5 and the nature of the low-energy excitations still remain controversial. The necessary steps towards solving these problems include (i)

an acquisition of precise high resolution experimental data on the properties of new low-temperature infrared and Raman modes in all the principal polarizations and (ii) a theoretical analysis of the properties of modes folded into the Brillouin zone (BZ) center of the LT-phase from different BZ-points of the paraphase.

The present work is devoted to the detailed high-resolution FIR transmission study of the frequencies, widths, and shapes of additional low-temperature modes of α' - NaV_2O_5 for $T \leq T_c$ in $\mathbf{E} \parallel \mathbf{a}$, $\mathbf{E} \parallel \mathbf{b}$, and $\mathbf{E} \parallel \mathbf{c}$ polarizations. To understand, at least qualitatively, polarization properties, splittings, and temperature behavior of the folded modes, we perform lattice dynamical calculations of the phonon dispersion curves throughout the Brillouin zone of the paraphase and of frequency changes due to lattice distortion and charge ordering below T_c . Possible manifestation of magnetic excitations and of the interaction between lattice, charge, and spin excitations in the FIR spectra are discussed.

II. EXPERIMENT

Samples of stoichiometric α' - NaV_2O_5 used in this study were grown by a melt growth method using NaVO_3 as a flux [30]. The process resulted in single crystals with dimensions from $1 \times 5 \times 0.5$ mm to $3 \times 17.3 \times 1.6$ mm along the a -, b -, and c -axes, respectively. Crystals from different batches were used. For transmission measurements in the $\mathbf{k} \parallel \mathbf{c}$, $\mathbf{E} \parallel \mathbf{a}$ or $\mathbf{E} \parallel \mathbf{b}$ configurations, we prepared four thin samples cleaved perpendicular to the c -axis. Their thicknesses were 111, 45, 14, and 6 μm . For the measurements in the $\mathbf{k} \parallel \mathbf{a}$, $\mathbf{E} \parallel \mathbf{c}$ or $\mathbf{E} \parallel \mathbf{b}$ geometries, two samples were used. One of them was 1.3 mm thick along the a -axis (sample 2). The other one was covered with epoxy and then polished to the thickness of 150 μm (sample 1). The samples were checked by X-ray diffraction, magnetization, and ESR measurements. They exhibited a sharp transition at about 34 K.

The transmittance spectra in a polarized light incident normally to the sample surface were measured in the spectral range 25–2000 cm^{-1} at a resolution 0.05–1.0 cm^{-1} using a BOMEM DA3.002 Fourier transform spectrometer equipped with a helium-vapor optical cryostat. Samples were mounted to a specially constructed cryostat inset that partially compensated thermal variations of the cryostat length. The temperature of the sample varied from 300 to 6 K and was stabilized with the precision of ± 0.1 K. At each temperature, a reference spectrum was taken. For the case of sample 1 measured in $\mathbf{E} \parallel \mathbf{c}$ polarization, transmittance is given relative to the layer of epoxy having the same thickness as the sample. Precision of the experimental line position was 0.05–0.5 cm^{-1} , depending on a particular line. Precise absolute wave number scale is an intrinsic property of Fourier transform spectroscopy.

III. RESULTS

Fig. 2 shows FIR polarized transmittance in the spectral range from 55 to 350 cm^{-1} for α' - NaV_2O_5 at temperatures above and below T_c . At $T \simeq 40$ K $> T_c$ in the displayed frequency range we found two phonon lines ($\omega_{TO} = 178$ and 225 cm^{-1}) in $\mathbf{E} \parallel \mathbf{b}$ polarization (for the discussion of the 215 cm^{-1} line see Ref. [5]); three strongly asymmetric phonon peaks at 90, 140, and 254 cm^{-1} visible on a strong absorption background in $\mathbf{E} \parallel \mathbf{a}$ polarization; two strong phonon lines with $\omega_{TO} = 163$ and 180 cm^{-1} , $\omega_{LO} = 169$ and 215 cm^{-1} (compare with $\omega_{TO} = 162$ and 179 cm^{-1} , $\omega_{LO} = 165$ and 212 cm^{-1} as determined from FIR reflectance spectra at room temperature [5]) and an absorption peak at 282 cm^{-1} in $\mathbf{E} \parallel \mathbf{c}$ polarization. This peak can be assigned to a missing B_{1u} phonon placed at 298 cm^{-1} by lattice dynamics calculations for the high-temperature (HT)-phase [5] and not observed in FIR reflectance spectra [5,26].

A broad absorption band centered at about 320 cm^{-1} is present in $\mathbf{E} \parallel \mathbf{a}$ spectrum (see also [20,31,32]). One can clearly see it in Fig. 2a where the transmittance of a 14 μm thick sample is almost zero near this frequency. No broad-band absorption of a comparable intensity exist in $\mathbf{E} \parallel \mathbf{b}$ (Fig. 2b) and $\mathbf{E} \parallel \mathbf{c}$ (Fig. 2c) polarizations (note that Figs. 2a and 2b refer to the 14 μm thick sample, while Fig. 2c represents the spectra of a 150 μm thick sample). The a -polarized FIR absorption continuum extends to about 1500 cm^{-1} and consists of two bands centered at 300 and 1100 cm^{-1} [31,5,32].

Drastic changes occur in the spectra of NaV_2O_5 at the transition temperature. First, the long-wavelength part of the broad-band absorption in $\mathbf{E} \parallel \mathbf{a}$ polarization decreases markedly, the sample becomes more transparent (see Fig. 2a). The changes of transmittance near the 178 cm^{-1} phonon line in $\mathbf{E} \parallel \mathbf{b}$ polarization are caused by a sharp narrowing of this phonon below T_c . A special study is necessary to clarify the question, whether the changes of background transmittance observed in $\mathbf{E} \parallel \mathbf{c}$ polarization can be explained by a similar reason, namely, by the changes of regular phonons 162, 179, and 282 cm^{-1} below the transition temperature, or there is a weak broad-band absorption that diminishes below T_c . The spectra modeling (see below) has shown that, indeed, a weak broad absorption band that bleaches below T_c is present in $\mathbf{E} \parallel \mathbf{c}$ polarization. The measured absorption coefficient at the frequency 115 cm^{-1} is $\kappa(\omega = 115 \text{ cm}^{-1}) = 20 \text{ cm}^{-1}$. To compare, for the $\mathbf{E} \parallel \mathbf{a}$ polarized broad-band absorption $\kappa(\omega = 115 \text{ cm}^{-1}) = 400 \text{ cm}^{-1}$.

Second, the shape of asymmetric peaks at 90 and 140 cm^{-1} in $\mathbf{E} \parallel \mathbf{a}$ spectrum changes to symmetric. Third, numerous new spectral features appear below T_c in $\mathbf{E} \parallel \mathbf{a}$, $\mathbf{E} \parallel \mathbf{b}$, and $\mathbf{E} \parallel \mathbf{c}$ spectra. The first two phenomena were already discussed in our earlier publication [20]. We have attributed a broad band in $\mathbf{E} \parallel \mathbf{a}$ polarization to two-spinon absorption, the asymmetric line shape being due to Fano-type resonance between lattice vibrations and a two-spinon continuum. The opening of a gap in the magnetic excitation spectrum below T_c leads to a vanishing of a low-frequency continuum and to the appropriate transformation of the line shapes. Subsequent structure redetermination for the HT phase of α' - NaV_2O_5 [2–5] does not, however, allow to ascribe $\mathbf{E} \parallel \mathbf{a}$ polarized spectral continuum to a pure two-spinon absorption. Symmetry considerations show that for both HT- and LT-structure of α' - NaV_2O_5 the two-spinon (two-magnon) absorption is allowed only in $\mathbf{E} \parallel \mathbf{c}$ polarization [33,34]. Probably, a weak FIR absorption background observed in this polarization results just from the two-spinon absorption. In that case, the observed diminishing of this absorption in the low-frequency region of $\mathbf{E} \parallel \mathbf{c}$ spectra would correspond to the opening of a gap in the magnetic excitation spectrum below T_c and also one would expect to observe the magnetic bound states, if any, just in $\mathbf{E} \parallel \mathbf{c}$ polarization. As for the $\mathbf{E} \parallel \mathbf{a}$ polarized low-frequency continuum, it could be formed by two spinons and one low-energy charge excitation, as has been proposed recently by Khomskii et al. in their paper on the spin-isospin model of α' - NaV_2O_5 [35].

In what follows, we concentrate our attention on the spectral lines that appear below T_c .

A. New spectral lines

Numerous new spectral lines appear in transmittance spectra below $T_c \simeq 34$ K and grow in intensity upon cooling the sample. For the spectral region 50–350 cm^{-1} they are marked by arrows in Fig. 2. Figs. 3–5 show some examples of the $\mathbf{E} \parallel \mathbf{a}$, $\mathbf{E} \parallel \mathbf{b}$, and $\mathbf{E} \parallel \mathbf{c}$ absorbance difference spectra $\alpha(T) - \alpha(37\text{K})$ for several temperatures. Here, the absorbance is defined by $\alpha = -\log_{10} Tr/d$, where Tr is the transmittance of a d cm thick sample.

The temperature behavior of the majority of new lines is characterized by an appreciable broadening and small (0.2–2 cm^{-1}) but clearly detectable shifts near T_c (see Figs. 6, 7). It should be mentioned that the vibrational lines that exist both below and above T_c also broaden and shift when approaching T_c from below (see insets of Fig. 6). Positions, widths, and oscillator strengths of the observed spectral lines that appear below T_c are listed in Table I.

These parameters were obtained from the following fitting procedure. The experimental transmittance spectrum at normal incidence was approximated by the expression [36]

$$Tr = \left| \frac{4\sqrt{\varepsilon}}{(\sqrt{\varepsilon} + 1)^2 e^{-i\beta d} - (\sqrt{\varepsilon} - 1)^2 e^{i\beta d}} \right|^2, \quad (1)$$

$$\beta = 2\pi\omega\sqrt{\varepsilon}$$

in the case of clearly visible interference pattern, or by the expression

$$Tr = (1 - \mathcal{R})^2 e^{-\kappa d} \quad (2)$$

in the absence of interference within the sample. Here

$$\mathcal{R} = \left| \frac{\sqrt{\varepsilon} - 1}{\sqrt{\varepsilon} + 1} \right|^2 \quad (3)$$

is the reflectivity of one surface,

$$\kappa = 4\pi\omega \text{Im}\sqrt{\varepsilon} \quad (4)$$

is the absorption coefficient. The dielectric function $\varepsilon(\omega)$ was represented as a sum of contributions from N noninteracting oscillators

$$\varepsilon = \varepsilon_\infty + \sum_{j=1}^N \frac{4\pi f_j \omega_j^2}{\omega_j^2 - \omega^2 - i\gamma_j \omega}, \quad (5)$$

where ε_∞ is the high-frequency dielectric constant, ω_j , γ_j , and f_j are the frequency, the damping constant, and the oscillator strength of the j -th oscillator. First of all, the calculated spectrum was fitted to the experimental one at

$T=37$ K, just above the temperature of the phase transition, starting from the room temperature values determined earlier in our work [5]. The fitting to the low-temperature ($T \simeq 10$ K) spectrum was performed in two steps. First, changes of the phonons that exist both in HT- and LT-phases were taken into account and, then, new oscillators were introduced.

It should be noted that we could not study several spectral regions because of a too strong absorption of either the sample or mylar windows of our cryostat. In particular, the lines at 718 cm^{-1} are only partially seen, being too close to a strong absorption band of mylar. Results of the $\mathbf{E} \parallel \mathbf{c}$, $\mathbf{k} \parallel \mathbf{a}$ measurements refer to the $150 \mu\text{m}$ thick sample. We were able to detect the lowest frequency lines also in the 1.3 mm thick sample. Their positions are indicated in brackets in Table I.

Fig. 8 shows the temperature dependence of the normalised oscillator strength of the modes 101.4 and 111.7 cm^{-1} ($\mathbf{E} \parallel \mathbf{b}$ polarization); 126.7 cm^{-1} ($\mathbf{E} \parallel \mathbf{a}$); $70, 106.9, 124.7, 133.1,$ and 140 cm^{-1} ($\mathbf{E} \parallel \mathbf{c}$). The data on the 101.4 and 111.7 cm^{-1} modes summarize a very detailed study of two samples with the thicknesses $d_1 = 14 \mu\text{m}$ and $d_2 = 111 \mu\text{m}$.

The intensity of the $101.4, 126.7,$ and 140 cm^{-1} modes follows the same temperature dependence as the intensity of new X-ray reflections corresponding to the doubling (a, b) and quadrupling (c) of the lattice constants [10] (also shown in Fig. 8). This dependence is characterized by a steep rise just below T_c and a saturation below ~ 22 K. The majority of the observed new lines behave like that, while several ones (in particular, the lines $91.2, 145.0, 145.7, 157.2,$ and 451.1 cm^{-1} in $\mathbf{E} \parallel \mathbf{a}$, 111.7 cm^{-1} in $\mathbf{E} \parallel \mathbf{b}$, $70, 106.9, 126.7,$ and 133.1 cm^{-1} in $\mathbf{E} \parallel \mathbf{c}$) demonstrate a more slow growth of intensity below T_c and a saturation at lower temperatures. We could not measure reliably the intensity dependence of the very weak feature at about 133 cm^{-1} in $\mathbf{E} \parallel \mathbf{c}$ polarization but it seems to grow in the slowest way among all the studied modes and to follow the same temperature dependence as the spin-gap mode observed in optical ESR measurements [37] (also shown in Fig. 8).

B. Factor-group analysis ($Fmm2$). Brillouin zone folding for different proposed low-temperature structures.

According to the recent X-ray diffraction work [6,14,15], the structure of the low-temperature phase of α' - NaV_2O_5 is face-centered, with $Fmm2$ space group on the $2a \times 2b \times 4c$ supercell. The primitive cell corresponding to the translation vectors $(a, 0, 2c)$, $(0, b, 2c)$, and $(a, b, 0)$ contains 64 atoms and, hence, there are 189 optical vibrational modes. Table II lists the Wyckoff positions of atoms in the $Fmm2$ supercell [6] and in the $Pmnm$ basic structure [2]. The corresponding local symmetries are also indicated. These positions yield the following irreducible representations of the vibrational modes at the Brillouin zone center of the $Fmm2$ LT-structure [38]:

$$\begin{aligned} C_1 &: 3A_1 + 3A_2 + 3B_1 + 3B_2 \\ C_{2v} &: A_1 + B_1 + B_2 \\ C_s^{xz} &: 2A_1 + A_2 + 2B_1 + B_2 \\ C_s^{yz} &: 2A_1 + A_2 + B_1 + 2B_2 \\ C_2 &: A_1 + A_2 + 2B_1 + 2B_2. \end{aligned}$$

Multiplying the representations given above by the number of different positions of the appropriate symmetry, summing them, and subtracting acoustic modes ($A_1 + B_1 + B_2$), we obtain the following optical vibrational modes:

$$\Gamma_{\text{NaV}_2\text{O}_5}^{\text{vib}}(Fmm2) = 55A_1(aa, bb, cc; E \parallel c) + 36A_2(ab) + 55B_1(ac; E \parallel a) + 43B_2(bc; E \parallel b).$$

153 modes (A_1, B_1, B_2) are both Raman and IR active, while $36A_2$ modes are allowed only in Raman scattering.

More information on the transition-induced vibrational modes, in particular, on the distribution of their frequencies, can be obtained from the analysis of the BZ folding at the structural phase transition. We have constructed the Brillouin zones for the $Pmnm$ HT-structure (it is shown in Fig. 9), for the $Fmm2$ LT-structure, and also for the other proposed LT-structures and analysed what points of the BZ of the paraphase fold into the new zone center and thus become optically active. Results of this analysis are represented in Table III.

In the case of $Fmm2$ low-temperature structure, the two Z -points $(0, 0, \pm \frac{1}{2})$ of the paraphase and the eight Q -points of the type $(\frac{1}{2}, \frac{1}{2}, \frac{1}{4})$ deliver 48 singlets $16A_1 + 6A_2 + 16B_1 + 10B_2$ (compatible with $(8Z_1 + 8Z_2) + (3Z_3 + 3Z_4) + (8Z_5 + 8Z_6) + (5Z_7 + 5Z_8)$ irreducible representations of the symmetry group of the Z -point) and, respectively, 24 quadruplets $12(2A_1 + 2A_2) + 12(2B_1 + 2B_2)$ (compatible with Q_1 and Q_2 doublets of the Q -point) to the BZ center of the LT phase. They join $15A_1 + 6A_2 + 15B_1 + 9B_2$ singlet vibrational modes that originate from, correspondingly, $(7B_{1u} + 8A_g) + (3A_u + 3B_{1g}) + (7B_{3u} + 8B_{2g}) + (4B_{2u} + 5B_{3g})$ vibrations of the BZ center (Γ -point) of the paraphase. Because of a degeneracy of the Q -point folded modes, the number of additional frequencies observed below T_c should be not so high as it followed from a simple factor-group analysis (namely, 72 instead of $189 - 45 = 144$).

In the case of the face-centered structures $Ccc2$, $C2/c$, or $C2$, there are 128 atoms in the primitive cell and, thus, 381 optical modes. In addition to the just mentioned BZ points Z and Q , the Λ , S , and R points also fold into the zone center delivering 96 additional doublets. A lattice distortion in the LT-phase lifts a degeneracy of folded quadruplets or quadruplets and doublets and causes their splitting. We shall consider the polarization properties of the split components in the section IVA.

C. Lattice dynamics calculations

We consider the lattice dynamics of α' - NaV_2O_5 in the framework of the rigid-ion model. The model incorporates long-range Coulomb interactions and short-range interactions described by Born-Mayer potentials. The model parameters were obtained in Ref. [5] by fitting to the HT-phase zone-center frequencies measured by optical techniques. In the present work, we use them to calculate the phonon dispersion curves throughout the Brillouin zone of the paraphase. As an example, Fig. 10 displays the calculated dispersion curves along the closed path $\Gamma(000) - \Lambda(00\frac{1}{4}) - Z(00\frac{1}{2}) - R(\frac{1}{2}\frac{1}{2}\frac{1}{2}) - Q(\frac{1}{2}\frac{1}{2}\frac{1}{4}) - S(\frac{1}{2}\frac{1}{2}0) - \Gamma(000)$ in the BZ of the high-temperature $Pm\bar{m}n$ structure for the two highest-frequency Davydov doublets $B_{3u} - B_{2g}$ and $B_{1u} - A_g$ originating from the stretching vanadium-apical oxygen vibration. We do not show here the rest of 48 phonon branches. Most of them exhibit pronounced slopes and complicated interactions. Many (but not all) of the dispersion curves along the Γ - Z direction are rather flat, reflecting more weak forces between layers in comparison with those inside a layer. However, only 12 out of 45 optical branches show a dispersion less than 6 cm^{-1} (6 cm^{-1} is a maximum line-width among the observed folded modes), and so the phonon spectrum of the LT-phase cannot be described in the framework of one layer, as has been proposed in Ref. [19].

Our lattice dynamical model neglects electronic polarization and does not take into account three-body forces that strongly affect the frequencies of bending vibrations. Because of that, there are several large discrepancies (50 – 80 cm^{-1}) between the calculated and observed zone-center phonon frequencies of the high-temperature $Pm\bar{m}n$ structure [5] and one cannot expect a good quantitative description of phonon frequencies throughout the Brillouin zone. (It should be mentioned, however, that the sound velocities determined from the slope of the acoustic branches along the ladders (the b -axis) at $k = 0$, $v = (\frac{d\omega}{dk})_{k=0}$, $v_l = 7.0 \cdot 10^5 \text{ cm/s}$, $v_t^{(1)} = 4.6 \cdot 10^5 \text{ cm/s}$, $v_t^{(2)} = 3.3 \cdot 10^5 \text{ cm/s}$, are in good agreement with the experimentally measured values $v_l = 6.5 \cdot 10^5 \text{ cm/s}$, $v_t^{(1)} = 4.2 \cdot 10^5 \text{ cm/s}$, $v_t^{(2)} = 2.6 \cdot 10^5 \text{ cm/s}$ [12].)

Though being crude, this simple rigid-ion model gives possibility to analyze, at least qualitatively, the main properties of the folded phonon modes in the low-temperature phase of α' - NaV_2O_5 . In particular, to follow the temperature shifts of the normal mode frequencies at temperatures near T_c , we have performed calculations in the framework of $Fmm2$ LT-structure, using the atomic coordinates from the structural work [6] and taking into account the charge redistribution. Three cases have been considered, namely, (i) lattice deformation ignored, redistributed charges of vanadium ions in the modulated ladders, $V^{4.5\pm\delta}$ with $\delta = 0.05$; (ii) lattice deformation ten times smaller than measured by X-ray diffraction at 15 K in Ref. [6], $\delta = 0.05$; (iii) the same as (ii) but $\delta = 0.1$. These calculations involved the numerical diagonalization of the dynamical matrix with dimensions 192×192 that was constructed using the same non-Coulomb force constants as in the paraphase. The main results of calculations are as follows.

1) The soft acoustic mode at the $(0, 0, \frac{1}{2})$ point of the BZ of the paraphase [5] becomes unstable under redistribution of the vanadium charge density alone, not taking into account the lattice distortion.

2) Both lattice distortion and charge disproportion cause normal mode frequency shifts and splitting of quadruplets (into $2A_1 + 2A_2$ or $2B_1 + 2B_2$ doublets), due to induced changes of the dynamical matrix. For different modes, displacements of atoms towards their new equilibrium positions and charge redistribution have effects upon frequencies either in the same or in the opposite direction. The shifts of “hard” singlet modes and splitting of quadruplets amount to 0.01–3% of their frequency.

IV. DISCUSSION

A. Splitting of the folded phonon modes

First of all, we put the question whether it is possible to explain the number and polarization properties of the additional low-temperature modes of α' - NaV_2O_5 supposing all of them to be vibrational folded modes of a dimerized lattice. Fourfold degeneracy of modes folded from the BZ Q -point at the phase transition determines some important peculiarities of the low-temperature vibrational spectrum of α' - NaV_2O_5 . We shall discuss them assuming, first, the $Fmm2$ group for the low-temperature structure [6,14,15]. In this case, Q_2 -quadruplets should manifest themselves as

$2B_1 + 2B_2$ pairs of doublets having close frequencies in $\mathbf{E} \parallel \mathbf{a}$ and $\mathbf{E} \parallel \mathbf{b}$ FIR spectra. For the two narrow additional low-temperature modes, namely, for the lines at about 101.5 and 127 cm^{-1} we really observe a gradual splitting into such doublets upon lowering the temperature (see Figs. 3,4,7). We suppose that the observed additional FIR lines with coincident or nearly coincident frequencies in $\mathbf{E} \parallel \mathbf{a}$ and $\mathbf{E} \parallel \mathbf{b}$ spectra correspond to unresolved $2B_1 + 2B_2$ doublets originating from Q_2 quadruplets. We place them into the lower right part of Table IV, together with Raman data from the literature. Note, that the frequency differences between 199.0 cm^{-1} ($\mathbf{E} \parallel \mathbf{a}$) and 199.5 cm^{-1} ($\mathbf{E} \parallel \mathbf{b}$) lines and between 959.7 cm^{-1} ($\mathbf{E} \parallel \mathbf{a}$) and 959.2 cm^{-1} ($\mathbf{E} \parallel \mathbf{b}$) lines are beyond the error limit of our high resolution measurements.

Q_1 -quadruplets should split into $2A_1 + 2A_2$ pairs of doublets. A_1 modes are observed in $\mathbf{E} \parallel \mathbf{c}$ polarization, while A_2 modes are silent in the IR spectra (but allowed in the (ab) Raman spectra). All the $\mathbf{E} \parallel \mathbf{c}$ modes are rather broad and we never observed a reliably resolved doublet structure. However, the shape of the lowest frequency mode near 70 cm^{-1} ($\mathbf{E} \parallel \mathbf{c}$) suggests a doublet structure (see Fig. 11). We have performed a fitting of the measured spectrum by the expressions (2)–(5) assuming a contribution from (i) one oscillator and (ii) two oscillators. Fig. 11 clearly demonstrates a much better result in the case of two oscillators. A doublet structure of the corresponding Raman A_1 -line has been reported in Ref. [39]. A_1 and A_2 Raman modes with coincident or close frequencies are listed in the lower left part of Table IV. So, the lower part of Table IV contains the LT modes that could originate from the BZ Q -point of the paraphase. In that case, 7 out of 12 Q_1 and 10 out of 12 Q_2 quadruplets are observed. Upper part of Table IV lists the rest of the observed additional LT modes from our measurements and from the literature. They could come from the Z-point, so that 10 out of 16 A_1 , 3 out of 6 A_2 , 11 out of 16 B_1 , and 3 out of 10 B_2 modes folded from the Z-point are observed. Raman and FIR modes that coincide in frequency within the absolute precision of Raman measurements (typically, $\pm 2 \text{ cm}^{-1}$) are put into the same line of Table IV.

Thus, the number and polarization properties of the additional modes that appear below the temperature of the phase transition in α' - NaV_2O_5 do not contradict their assignment to folded modes of the distorted $Fmm2$ structure.

Now we compare in more detail the experimental results to the results of lattice dynamics calculations for the frequency range displayed in Fig. 10. Table V lists the calculated frequencies of the Γ -point TO and LO modes and Z- and Q -point modes relevant to the zone folding in the case of $Fmm2$ LT-structure. All the experimentally observed modes in this frequency range can be reasonably ascribed to the modes of the $Fmm2$ structure (see columns 3 and 4 of Table V). The modes 948 (A_1) and 948 cm^{-1} (A_2) with coincident frequencies in A_1 and A_2 Raman spectra and two clearly different infrared modes 959.7 (B_1) and 959.2 cm^{-1} (B_2) in $\mathbf{E} \parallel \mathbf{a}$ and $\mathbf{E} \parallel \mathbf{b}$ polarizations should correspond to unresolved $2A_1$ and $2A_2$ and, respectively, $2B_1$ and $2B_2$ doublets folded from the Q -point. According to our lattice dynamics calculations (for the case (iii) of the Section IIIC), Q_1 (969 cm^{-1}) and Q_2 (973 cm^{-1}) quadruplets (see Fig. 10) split into $2A_1$ (967.8–970.3 cm^{-1}) and $2A_2$ (969.3–969.4 cm^{-1}) and, respectively, $2B_1$ (974.8–977.0 cm^{-1}) and $2B_2$ (973.5–973.6 cm^{-1}) doublets. These splittings are within the limits of the linewidths.

If the space group for the LT-phase of α' - NaV_2O_5 were a subgroup of $Fmm2$ (e.g., $Ccc2$ [17,18]), 48 additional doublets $16 \times 2A_1 + 6 \times 2A_2 + 16 \times 2B_1 + 10 \times 2B_2$ from the Λ point would appear independently in the spectra of different symmetries and also one would expect additional 96 singlets $24(A_1 + A_2)$ and $24(B_1 + B_2)$ with close frequencies in A_1 and A_2 and B_1 and B_2 spectra, originating from the folded S - and R -doublets. Domains due to oblique charge ordering pattern possible for a zigzag charge order in every ladder in the space group $Ccc2$ [17,32] would not affect the direction of the orthorhombic a- and b-axes and, thus, polarization properties of vibrational modes. Experimental data on the new LT-modes do not contradict both $Fmm2$ and $Ccc2$ symmetries. However, while in the first case one has to admit that 27 new frequencies remained unobserved, in the latter one this quantity grows up to 123. In both cases, close or coincident frequencies in A_1 and A_2 and B_1 and B_2 spectra are naturally explained by their origin from the folded BZ Q -point ($Fmm2$) or Q , Λ , S , and R -points ($Ccc2$). A possible monoclinic distortion (space groups $C2$ [18] or $C2/c$ [19]) would violate the $\mathbf{E} \parallel \mathbf{a}$ or $\mathbf{E} \parallel \mathbf{b}$ FIR selection rules, as well as Raman selection rules. Probably, the growing contribution of the A_{1g} modes 530 and 304 cm^{-1} to the (ab) Raman spectrum for the temperatures below $\sim 100 \text{ K}$ observed in Ref. [28] is just because of such a distortion.

At the first glance, LT modes fit the $C2/c$ centrosymmetric group proposed in Ref. [19]. In particular, in the case of $C2/c$ group Q_2 -quadruplets would split into $2B_u(\mathbf{E} \parallel \mathbf{a}, \mathbf{E} \parallel \mathbf{b}) + 2B_g(ac, bc)$ doublets. Such a scenario seems to describe better the experimental data (see the lower right part of Table IV). However, the frequency differences between the observed FIR and Raman modes are within the precision of Raman measurements.

To summarize, it is not possible to chose between the proposed space symmetry groups for the low-temperature crystal structure of α' - NaV_2O_5 on purely spectroscopic grounds. The number and polarization properties of all the observed new LT modes in α' - NaV_2O_5 can be reasonably described within the conception of folded vibrational modes of the dimerized $Fmm2$ crystal structure. Observed FIR doublets and close frequencies in different polarizations are naturally explained by their origin from the Q -point modes folded into the zone center. Prior to analyse the temperature dependences of frequencies and widths of new modes and to discuss alternative interpretations, we note that published FIR [20,23,26,5,32] and Raman [9,21,27,28,19,39,29] data agree with each other, within the precision of measurements (typically, $\pm 0.5 \text{ cm}^{-1}$ for FIR and $\pm 1.5 \text{ cm}^{-1}$ for Raman measurements).

B. Magnetic bound states?

As we mentioned in Section IIIA, three of the observed new low-temperature modes, namely, modes near 70, 107, and 133 cm^{-1} in $\mathbf{E} \parallel \mathbf{c}$ polarization, have different frequencies in different samples (see Table IV). These modes and the mode near 125 cm^{-1} ($\mathbf{E} \parallel \mathbf{c}$) demonstrate unusually large broadening, shift, and loss of intensity upon heating (see Figs. 6, 8). All these modes were observed also in Raman scattering (see Table IV), exhibiting the same properties as their infrared counterparts.

In Refs. [21,39], Raman modes near 65 and 132 cm^{-1} have been assigned to one- and two-magnon scattering processes, respectively. The frequency 64–70 cm^{-1} of the lowest-frequency sharp feature in FIR and Raman spectra below T_c corresponds well to the size of the gap $\Delta_0 = 8.13 \text{ meV} = 65.6 \text{ cm}^{-1}$ at $\mathbf{k} = \mathbf{0}$ obtained from submillimeter ESR measurements [37]. The transitions between the singlet ground state and the excited triplet state are forbidden ($\Delta S = 1$). The Dzyaloshinsky-Moria (DM) interaction with DM vector along the c -axis breaks the selection rule for ESR (and FIR) $\mathbf{E} \parallel \mathbf{c}$ transitions in α' - NaV_2O_5 [37,34]. Recently, it has been shown theoretically [34] that for α' - NaV_2O_5 the DM interaction results in finite Raman cross-section for both one- and two-magnon scattering processes. A single-magnon Raman line of this type should show no splitting in an external magnetic field parallel to the c -axis but should split into two branches for a field perpendicular to the c -axis. The authors of Ref. [28] communicated that the 67 cm^{-1} Raman line neither shifts nor splits nor even broadens in a magnetic field up to 7 T. They have attributed this line and the 107 and 134 cm^{-1} Raman modes to magnetic singlet bound states, on the basis of (i) the temperature dependence of the intensity, frequency shift, and linewidth, and (ii) the frequency dependence on a sample quality. All the three modes rapidly lose their intensity, soften and broaden on approaching T_c from below [27,28]. It is worth mentioning that very recently two more Raman modes with similar properties have been reported (namely, 86 and 126 cm^{-1} modes in (ab) geometry) [29]. To our opinion, the interpretation of the 67, 107, and 134 cm^{-1} modes as magnetic bound states does not follow unambiguously from the above mentioned arguments.

One of the main arguments in favor of considering 67, 107, and 134 cm^{-1} Raman modes as magnetic bound states was a slow increase of their intensity upon cooling. For comparison, the intensities of the folded phonon Raman modes at 202, 246, and 948 cm^{-1} rose sharply below T_c and then saturated. However, our measurements show that many of the transition-induced modes demonstrate a slow growth of intensity upon cooling below T_c . Among them, the considered mode near 107 cm^{-1} ($\mathbf{E} \parallel \mathbf{c}$) and the folded phonon mode 111.7 cm^{-1} ($\mathbf{E} \parallel \mathbf{b}$) behave in the same way (see Fig. 8).

Different temperature dependences of the type $(T_c - T)^{2n\beta}$ (here β is the critical index of the order parameter; $n = 1, 2, 3$) for the intensities, frequencies and widths of the folded modes in the vicinity of a structural phase transition have been reported and analysed by Petzelt and Dvořák [40], taking into account anharmonic couplings between modes. In α' - NaV_2O_5 , as we show below, a mere charge disproportion may lead to the $(T_c - T)^{2n\beta}$, $n > 1$, intensity dependence for a folded phonon mode below T_c , even in the harmonic approximation.

Intensity of a FIR spectral line is proportional to a square of the electric dipole moment of a primitive cell induced by the respective vibrational mode. The dipole moment may be represented as a sum of products of effective atomic charges and corresponding displacements of Bravais sublattices. A slow intensity dependence may be expected when the main contribution to the dipole moment comes from the charge disproportion terms that involve displacements renormalized by the order parameter. Let us consider, for example, the z -component of the electric dipole moment due to displacements of vanadium ions that transform according to the A_1 representation of the factor group of the LT phase. The primitive cell of the $Fmm2$ structure contains eight $\text{V}^{4.5+}$ ions that form two rectangular plaquettes (fragments of nonmodulated ladders) in the neighboring ab -layers, four V^{4+} , and four V^{5+} ions on the rungs of the neighboring (left and right) modulated ladders (see Fig. 1). Normal modes that correspond to Z_1 , Z_2 , and Q_1^1 representations involve antiphase translations of $\text{V}^{4.5+}$ plaquettes along the c -axis and antiphase displacements of V^{5+} and V^{4+} ions along the same axis. At T_c , all the displacements have equal amplitudes, vanadium ions have equal charges, and the corresponding electric dipole moment is zero. At $T < T_c$, nonzero dipole moment appears due to different amplitudes of the plaquette translations and different amplitudes of $\text{V}^{4.5-\delta}$ and $\text{V}^{4.5+\delta}$ ions. Our calculations confirmed that, for some low frequency modes involving large amplitudes of vanadium ions vibrations, the effective electric dipole moment is determined mainly by the terms containing the charge disproportion δ and the differences between ion amplitudes at the temperatures T and T_c . These terms provide the $(T_c - T)^{4\beta}$ dependence of the FIR absorption. The same consideration is applicable to the Raman spectra where intensities are determined by electric polarizabilities of lattice modes.

Thus, a slow growth of the mode intensity below T_c is not a unique property of the spin-gap related excitations only. Furthermore, if we compare the intensities of the FIR new modes measured in this work with the integrated intensity of the spin-gap mode observed in optical ESR measurements [37], it is evident that only the 133 cm^{-1} mode follows the same temperature dependence as the gap-mode (see Fig. 8).

Now in Fig. 12 we compare the normalized magnetic gap energy, as observed in neutron scattering experiments [10],

and the normalized frequencies of the 70 and 106.9 cm^{-1} FIR modes. The latter change much more slowly on approaching T_c than the magnetic gap. We could not measure the frequency of the weak 133 cm^{-1} FIR mode below 24 K but the corresponding Raman mode practically does not shift within the interval of T/T_c from 0.2 to 0.88, as one can see from the spectra of Ref. [29]. Thus, the temperature dependence of the peak positions for the lines near 70, 107, and 124.7 cm^{-1} differ significantly from the dependence for the singlet-triplet gap, $\Delta(T)$, while the frequency of the Raman peak near 30 cm^{-1} corresponding to a magnetic bound state in CuGeO_3 followed the same temperature dependence as $\Delta(T)$ [41].

To summarize, the comparison between the temperature-dependent intensities of the transition-induced FIR modes and of the spin-gap mode show that the mode 133 cm^{-1} is the only one that could be considered as a magnetic bound state. However, the temperature dependence of its frequency contradicts this hypothesis. Thus, the assignment of the 70, 107, and 133 cm^{-1} modes to magnetic bound states seems to be wrong.

As an alternative interpretation we would propose folded phonon modes that strongly interact with charge and spin excitations. The interaction renormalizes the frequencies of phonons, causes mode broadening and softening near T_c . A sodium deficiency strongly influences magnetic (and charge) states which leads to a strong change of interaction parameters. This circumstance could explain the dependence of 70, 106, and 133 cm^{-1} mode frequencies on a sample quality. Our earlier observation on the x -dependent phonon frequencies in $\text{Na}_{1-x}\text{V}_2\text{O}_5$ [5] supports such an assumption. We observed a giant frequency shift of 30 cm^{-1} for one of the (aa) Raman modes. Namely, the 447 cm^{-1} mode ($x = 0$) moved to 477 cm^{-1} for $x = 0.15$. Simultaneously, the maximum of a broad-band scattering moved in the opposite direction, from 632 cm^{-1} for $x = 0$ to 562 cm^{-1} for $x = 0.15$. It was naturally to explain this change of the frequency difference between two Raman bands by a change of interaction between the corresponding excitations [5]. Though the exact nature of the broad band in the (aa) Raman geometry is not yet clear, it must be connected with low-frequency electronic excitations on the ladder rungs [28,35].

The interaction between spin, charge, and lattice degrees of freedom is an intrinsic property of α' - NaV_2O_5 . In sodium vanadate one d -electron belongs to two vanadium atoms which gives an additional electronic degree of freedom. The electron hopping amplitude along a ladder rung is significantly higher than the amplitudes of hopping along a ladder or between different ladders [2,8]. Zigzag charge ordering at low temperatures can be described as an antiferroelectric ordering of electric dipoles on the rungs of vanadium ladders [35]. As each electron carries the spin ($S=1/2$), charge and spin degrees of freedom are closely connected. To describe this situation, Mostovoy and Khomskii proposed a spin-isospin model and used it to show that the antiferroelectric charge ordering in the system of vanadium ladders opens a spin gap [42,35]. They argued that in α' - NaV_2O_5 the quasi-one-dimensional spin system is strongly coupled to a low-energy antiferroelectric mode (isospin mode) of the excitonic type and the observed charge ordering corresponds to the softening of this mode. The softening of the isospin excitation occurs at the wave vector of the superlattice structure appearing in the ordered phase [35], that is, at the Q -point ($\frac{1}{2}\frac{1}{2}\frac{1}{4}$). Low-energy vibrational excitations of the corresponding symmetry should strongly interact with the isospin mode. To understand a possible mechanism of such an interaction we refer to Fig. 13 showing atomic displacements for vanadium atoms in the lowest-frequency A_1 mode (at 136 cm^{-1} , according to our calculations) folded from the BZ Q -point into the zone center. Vibrations are mainly along the c -axis, vanadium atoms at the two ends of a rung move in antiphase, that is when the left atom approaches the apical oxygen, the right one moves away from it. Such a motion stimulates vanadium charge redistribution ($\text{V}^{4.5\pm\delta}$) [43] that corresponds just to a static picture of charge ordering.

By inspecting the experimental results summarized in Table I we notice that the lowest frequency A_1 -symmetry modes ($\mathbf{E} \parallel \mathbf{c}$) are about an order of magnitude broader than the lowest-frequency B_1 ($\mathbf{E} \parallel \mathbf{a}$) and B_2 ($\mathbf{E} \parallel \mathbf{b}$) modes even in the limit $T \rightarrow 0$. They have the ratio $\gamma/\omega \simeq 2 \div 6 \cdot 10^{-2}$ in comparison with $1 \div 3 \cdot 10^{-3}$ for B_1 and B_2 modes. Such a broadening could result from a decay of the low-frequency vibrations into isospin and spin excitations, due to the interaction with them. High-resolution neutron inelastic scattering experiments on the spin excitations of α' - NaV_2O_5 revealed the two branches associated with distinct energy gaps [44,45]. At the zone boundary ($\frac{1}{2}\frac{1}{2}0$) (as well as at the zone center) these gaps constitute 68.6 cm^{-1} [44] (67 cm^{-1} according to Ref. [45]) and 91.1 cm^{-1} [44] (87.8 cm^{-1} [45]). Keeping in mind the energy and momentum conservation laws, the following decay channels are possible: direct interaction with the zone center magnon or a decay into two zone boundary isospin excitations (for the 70 cm^{-1} mode), a decay into a zone boundary magnon (66 or 90 cm^{-1}) and the isospin excitation (for the 106 or 125 cm^{-1} modes). Such a process corresponds to a hopping of an electron along the ladder rung and a simultaneous spin-flip. In that case, the zone boundary isospin gap would constitute of about 35 cm^{-1} , in reasonable agreement with the theoretical estimates [35].

C. In search for a soft mode

The lattice dynamics calculations for the high-temperature phase of α' - NaV_2O_5 predicted a soft mode behavior of the transverse acoustic mode at the BZ boundary with $\mathbf{k} = (00\frac{1}{2})$. It was found to become unstable under charge redistribution below T_c . So, one could expect a doubling of the unit cell along the c -axis, as a precursor of the subsequent magnetic ordering with a dimerization along the a -, b -, and c -directions. We have to mention that two subsequent phase transitions within the temperature interval of 1 K have been communicated in Ref. [46].

The discussed soft mode corresponds to the irreducible representation Z_5 of the BZ $(00\frac{1}{2})$ point and it could be observed as a folded FIR mode in $\mathbf{E} \parallel \mathbf{a}$ polarization. We have thoroughly studied low-temperature a -polarized FIR transmittance spectra of $1\text{mm} \times 3\text{mm} \times 111\mu\text{m}$ sample of α' - NaV_2O_5 in the spectral range 20–138 cm^{-1} but failed to find a soft mode. Possibly, it has a frequency lower than 20 cm^{-1} at 6 K or its oscillator strength is too small. Another possibility would be that this soft mode is simply a property of our rather crude model of lattice dynamics.

The $\mathbf{E} \parallel \mathbf{c}$ polarized 70 and 107 cm^{-1} modes demonstrate the strongest observed softening toward T_c . But this softening is only of about 3 % and is, probably, connected with the interaction of lattice modes with magnetic and charge excitations, as discussed in the previous section. It looks like the true soft mode of the phase transition in α' - NaV_2O_5 is of electronic nature (low-energy antiferroelectric (isospin) mode [35]).

V. CONCLUSIONS

In summary, we report the temperature-dependent polarized high-resolution FIR transmission spectra of α' - NaV_2O_5 . The comparison with the results of neutron scattering and optical ESR measurements and the theoretical analysis of the properties of vibrational modes in a charge ordered state lead us to the conclusion that all the transition-induced new modes of α' - NaV_2O_5 can be completely described in terms of folded modes of a dimerized lattice.

Based on the present results, the widely accepted interpretation of several lowest-frequency new modes as magnetic bound states seems highly unlikely. As an alternative interpretation of 70, 106, 125, and 133 cm^{-1} spectral lines we suggest low-frequency lattice vibrations of an appropriate symmetry that strongly interact with charge and spin excitations at the BZ boundary of the high-temperature phase and fold into the zone center at the phase transition into a dimerized state.

Note: When this paper already was with editors be became aware of the work [47] where $\mathbf{E} \parallel \mathbf{c}$ transmittance of α' - NaV_2O_5 was measured and low-frequency transition-induced modes were reported to appear at 68, 106, and 124 cm^{-1} ($T = 4.2$ K) and not to change under the magnetic field up to 15 T.

ACKNOWLEDGEMENT

Useful discussions with A. N. Vasil'ev, A. I. Smirnov, and G. N. Zhizhin are acknowledged. We thank D. M. Shkrabo for modeling several spectra. We are grateful to P. van Loosdrecht for critically reading the manuscript. This work was supported by INTAS, grant No. 99-0155 and by the Russian Foundation for Basic Research, grant No. 01-02-16329.

-
- [1] M. Isobe and Y. Ueda, J. Phys. Soc. Jap. **65**, 1178 (1996).
 - [2] H. Smolinski, C. Gros, W. Weber, U. Peuchert, G. Roth, M. Weiden, and C. Geibel, Phys. Rev. Lett. **80**, 5164 (1998).
 - [3] A. Meetsma, J. L. de Boer, A. Damascelli, T. T. M. Palstra, J. Jegoudez, and A. Revcolevschi, Acta Cryst. C **54** 1558 (1998).
 - [4] H. G. von Schnering, Y. Grin, M. Kaupp, M. Somer, R. K. Kremer, O. Jepsen, T. Chatterji, and M. Weiden, Z. Kristallogr. **213**, 246 (1998).
 - [5] M. N. Popova, A. B. Sushkov, S. A. Golubchik, B. N. Mavrin, V. N. Denisov, B. Z. Malkin, A. I. Iskhakova, M. Isobe, and Y. Ueda, ZhETF **115**, 2170 (1999); [JETP **88**, 1186 (1999)].
 - [6] J. Lüdecke, A. Jobst, S. van Smaalen, E. Morr , C. Geibel, and H. G. Krane, Phys. Rev. Lett. **82**, 3633 (1999).
 - [7] T. Ohama, H. Yasuoka, M. Isobe, and Y. Ueda, Phys. Rev. B **59**, 3299 (1999).
 - [8] P. Horsch and F. Mack, Eur. Phys. J. B **5**, 367 (1998).
 - [9] M. Weiden, R. Hauptmann, C. Geibel, F. Steglich, M. Fisher, P. Lemmens, and G. Guntherodt, Z. Phys. B **103**, 1 (1997).

- [10] Y. Fujii, H. Nakao, T. Yoshihama et al., *J. Phys. Soc. Jap.* **66**, 326 (1997).
- [11] A. I. Smirnov, M. N. Popova, A. B. Sushkov, S. A. Golubchik, D. I. Khomskii, M. V. Mostovoy, A. N. Vasil'ev, M. Isobe, and Y. Ueda, *Phys. Rev. B* **59**, 14546 (1999).
- [12] H. Schvenk, S. Zherlitsyn, B. Lüthi, E. Morre, and C. Geibel, *Phys. Rev. B* **60**, 9194 (1999).
- [13] H. Nakao, K. Ohwada, N. Takesue, Y. Fujii, M. Isobe, Y. Ueda, M. v. Zimmermann, J. P. Hill, D. Gibbs, J. C. Woicik, I. Koyama, and Y. Murakami, *Phys. Rev. Lett.* **85**, 4349 (2000).
- [14] J. L. de Boer, A. M. Meetsma, J. Baas, and T. T. M. Palstra, *Phys. Rev. Lett.* **84**, 3962 (2000).
- [15] A. Bernert, T. Chatterji, P. Thalmeier, and P. Fulde, *cond-mat/0012327*.
- [16] S. van Smaalen and J. Lüdecke, *Europhys. Lett.* **49**, 250 (2000).
- [17] T. Ohama, A. Goto, T. Shimizu, E. Ninomiya, H. Sawa, M. Isobe, and Y. Ueda, *J. Phys. Soc. Jap.* **69**, 2751 (2000).
- [18] J. L. de Boer, G. Maris, A. M. Meetsma, J. Baas, and T. T. M. Palstra, *cond-mat/0008054*.
- [19] M. J. Konstantinović, Z. V. Popović, A. N. Vasil'ev, M. Isobe, and Y. Ueda, *Solid State Commun.* **112**, 397 (1999).
- [20] M. N. Popova, A. B. Sushkov, A. N. Vasil'ev, M. Isobe, and Y. Ueda, *Pis'ma v ZhETF* **65** 711 (1997) [*JETP Lett.* **65** 743 (1997)].
- [21] H. Kuroe, H. Seto, J. Sasaki, T. Sekine, M. Isobe, and Y. Ueda, *J. Phys. Soc. Japan* **67**, 2881 (1998).
- [22] M. Fischer, P. Lemmens, G. Güntherodt, M. Weiden, R. Hauptmann, C. Geibel, and F. Steglich, *Physica B* **244**, 76 (1998).
- [23] D. Smirnov, P. Millet, J. Leotin, D. Poilblanc, J. Riera, D. Augier, and P. Hansen, *Phys. Rev. B* **57**, R11035 (1998).
- [24] A. Damascelli, D. van der Marel, M. Grüninger, C. Pressura, T. T. M. Palstra, J. Jegoudez, and A. Revcolevschi, *Phys. Rev. Lett.* **81**, 918 (1998).
- [25] M. N. Popova, A. B. Sushkov, S. A. Golubchik, M. Isobe, and Y. Ueda, *Physica B* **284–286**, 1617 (2000).
- [26] D. Smirnov, J. Leotin, P. Millet, J. Jegoudez, and A. Revcolevschi, *Physica B* **259–261**, 992 (1999).
- [27] P. Lemmens, M. Fischer, G. Els, G. Güntherodt, A. S. Mishchenko, M. Weiden, R. Hauptmann, C. Geibel, and F. Steglich, *Phys. Rev. B* **58**, 14159 (1998).
- [28] M. Fischer, P. Lemmens, G. Els, G. Güntherodt, E. Ya. Sherman, E. Morré, C. Geibel, and F. Steglich, *Phys. Rev. B* **60**, 7284 (1999).
- [29] M. J. Konstantinović, J. C. Irwin, M. Isobe, and Y. Ueda, *cond-mat/0103453*.
- [30] M. Isobe, C. Kagami, and Y. Ueda, *J. Crystal Growth* **181**, 314 (1997).
- [31] S. A. Golubchik, M. Isobe, A. N. Ivlev, B. N. Mavrin, M. N. Popova, A. B. Sushkov, Y. Ueda, and A. N. Vasil'ev, *J. Phys. Soc. Japan* **66**, 4042 (1997).
- [32] A. Damascelli, C. Presura, D. van der Marel, J. Jegoudez, and A. Revcolevschi, *Phys. Rev. B* **61**, 2535 (2000).
- [33] T. Moriya, *J. Appl. Phys.* **39**, 1042 (1968).
- [34] R. Valenti, C. Gros, and W. Brenig, *Phys. Rev. B* **62**, 14164 (2000); *cond-mat/0006036*.
- [35] M. Mostovoy, J. Knoester, and D. Khomskii, *cond-mat/0009464*.
- [36] M. Born, E. Wolf, *Principles of optics*, 2nd ed. (Pergamon Press, Oxford, London, Edinburgh, New York, Paris, Frankfurt, 1964).
- [37] S. Luther, H. Nojiri, M. Motokawa, M. Isobe, and Y. Ueda, *J. Phys. Soc. Jpn* **67**, 3715 (1998); **69**, 2291 (2000).
- [38] D. L. Rousseau, R. P. Bauman, and S. P. S. Porto, *J. Raman Spectr.* **10**, 253 (1981).
- [39] M. J. Konstantinović, K. Ladavac, A. Belić, Z. V. Popović, A. N. Vasil'ev, M. Isobe, and Y. Ueda, *J. Phys.:Condens. Matter* **11**, 2103 (1999).
- [40] J. Petzelt and V. Dvořák, *J. Phys. C: Solid State Phys.* **9**, 1571 (1976).
- [41] H. Kuroe, T. Sekine, M. Hase, Y. Sasago, K. Uchinokura, H. Kojima, I. Tanaka, and Y. Shibuya, *Phys. Rev. B* **50**, 16468 (1994).
- [42] M. V. Mostovoy and D. I. Khomskii, *Solid State Commun.* **113**, 159 (2000).
- [43] E. Ya. Sherman, M. Fischer, P. Lemmens, P. H. M. van Loosdrecht, and G. Güntherodt, *Europhys. Lett.* **48**, 648 (1999).
- [44] T. Yosihama, M. Nishi, K. Nakajima, K. Kakurai, Y. Fujii, M. Isobe, C. Kagami, and Y. Ueda, *J. Phys. Soc. Japan* **67**, 744 (1998).
- [45] B. Grenier, O. Cepas, L. P. Regnault, J. E. Lorenzo, T. Ziman, J. P. Boucher, A. Hiess, T. Chatterji, J. Jegoudez, and A. Revcolevschi, *cond-mat/0007025*.
- [46] M. Köppen, D. Pankert, R. Hauptmann, M. Lang, M. Weiden, C. Geibel, and F. Steglich, *Phys. Rev. B* **57**, 8466 (1998).
- [47] K. Tahekana, T. Takamasu, G. Kido, M. Isobe, and Y. Ueda, *Physica B* **294–295**, 79 (2001).

TABLE I. Parameters at $T = 9$ K of the FIR absorption lines activated by the phase transition in α' - NaV_2O_5 . The frequencies of $\mathbf{E} \parallel \mathbf{c}$ modes in the sample 2 are given in brackets. Here ω_j is the mode frequency, γ_j is the damping constant, f_j is the oscillator strength.

| $\mathbf{E} \parallel \mathbf{a}$ | | | $\mathbf{E} \parallel \mathbf{b}$ | | | $\mathbf{E} \parallel \mathbf{c}$ | | |
|-----------------------------------|----------------------------|------------------|-----------------------------------|----------------------------|------------------|-----------------------------------|----------------------------|------------------|
| ω_j, cm^{-1} | γ_j, cm^{-1} | $10^4 \cdot f_j$ | ω_j, cm^{-1} | γ_j, cm^{-1} | $10^4 \cdot f_j$ | ω_j, cm^{-1} | γ_j, cm^{-1} | $10^4 \cdot f_j$ |
| 91.2 | 0.17 | 4.7 | 101.4 | 0.20 | 5.2 | 70.0 (67.5) | 4.5 | 33 |
| 101.4 | 0.24 | 8.0 | 111.7 | 0.24 | 1.2 | 106.9 (106.2) | 2.3 | 10 |
| 101.7 | 0.16 | 3.6 | 126.8 | 0.31 | 3.4 | 124.7 (124.7) | 1.0 | 1.6 |
| 125.6 | 0.24 | 0.4 | 127.5 | 0.33 | 9.0 | 133.1 (131.6) | 2.5 | 0.5 |
| 126.8 | 0.33 | 13.0 | 199.5 | 1.3 | 2.5 | 140.0 | 0.7 | 1.3 |
| 127.6 | 0.30 | 4.8 | 234.2 | 2.0 | 2.6 | 148.2 | 0.6 | 0.7 |
| 145.0 | 0.46 | 3.2 | 324.6 | 3.9 | 5.2 | 256.5 | 2.6 | 0.05 |
| 145.7 | 0.43 | 7.6 | 410.3 | 2.0 | 1.5 | 327.4 | 6.0 | 0.17 |
| 147.9 | 0.5 | 26 | 959.2 | 1.3 | 0.06 | | | |
| 157.2 | 0.3 | 0.8 | | | | | | |
| 199.0 | 1.8 | 46.2 | | | | | | |
| 410.4 | 4.3 | 26 | | | | | | |
| 451.1 | 2.9 | 3.7 | | | | | | |
| 959.7 | 1.5 | 0.4 | | | | | | |

TABLE II. Wyckoff positions of atoms in the elementary cells of α' - NaV_2O_5 above and below T_c . Figures before chemical symbols denote numbers of atoms of the same kind.

| $T > T_c, Pmmn$ [2] | | | | $T < T_c, Fmm2$ [6] | | | | |
|---------------------|------------------|---------------|------------|---------------------|---------------|-------|------------------|---------------|
| Atom | Wyckoff position | Site symmetry | Atom | Wyckoff position | Site symmetry | Atom | Wyckoff position | Site symmetry |
| 1 | V | $4f$ | C_s^{xz} | 2 | V1 | $16e$ | C_1 | |
| | | | | 4 | V2 | $8d$ | C_s^{xz} | |
| 1 | Na | $2b$ | C_{2v} | 4 | Na1 | $4a$ | C_{2v} | |
| | | | | 2 | Na2 | $8b$ | C_2 | |
| 1 | O1 | $2a$ | C_{2v} | 2 | O11 | $8c$ | C_s^{yz} | |
| | | | | 2 | O12 | $8d$ | C_s^{xz} | |
| 1 | O2 | $4f$ | C_s^{xz} | 2 | O21 | $16e$ | C_1 | |
| | | | | 4 | O22 | $8d$ | C_s^{xz} | |
| 1 | O3 | $4f$ | C_s^{xz} | 2 | O31 | $16e$ | C_1 | |
| | | | | 4 | O32 | $8d$ | C_s^{xz} | |

TABLE III. Number of atoms in a primitive cell n , number of BZ center optical vibrational modes N ; points in the BZ of the paraphase that fold into the zone center and corresponding optical modes in the cases of different proposed space groups for the distorted structure. m is the number of additional frequencies just below T_c .

| Space group | n | N | BZ points | Optical modes | m |
|--|-----|-----|-------------------------------|--|-----|
| $Fmm2$ [6,14,15] | 64 | 189 | Γ, Z, Q | $45\Gamma + 48Z + 24 \times 4Q$ | 72 |
| $Ccc2$ [17,18], $C2/c$ [19], and $C2$ [18] | 128 | 381 | $\Gamma, Z, Q, \Lambda, S, R$ | $45\Gamma + 48Z + 24 \times 4Q$ $+48 \times 2\Lambda + 24 \times 2S$ $+24 \times 2R$ | 168 |

TABLE IV. Additional low-temperature IR and Raman modes of α' - NaV_2O_5 . Figures in brackets refer to the second sample used in this work or in Ref. [28].

| A_1 | | A_2 | B_1 | | B_2 | |
|--------------------------------|-------------------------------------|-------------------------------------|--------------------------------|------------------|--------------------------------|------------------|
| IR $\mathbf{E} \parallel c$ | Raman (aa), (bb), (cc) | Raman (ab) | IR $\mathbf{E} \parallel a$ | Raman (ac) | IR $\mathbf{E} \parallel b$ | Raman (bc) |
| 107 (106) | 107 (103) ^a | 86 ^c | 91.2 | | 111.7 | |
| 140.0 | 140 ^b | | 125.6 | 116 ^e | 234.2 | |
| | 164 ^a | 159 ^b , 158 ^c | 145.1 | | | 354 ^e |
| * | 202 ^a | 422 ^{a,d} | 145.7 | | | |
| 256 | | | 147.9 | | | |
| | 296 ^b | | 157.2 | 157 ^f | | |
| 314 | | | * | 306 ^f | | |
| * | 394 ^a | | 374 ^g | | | |
| * | 650 ^a | | 451.1 | | | |
| * | 692 ^a | | 787.3 | | | |
| | | | [969 ^h] | | | |
| 70.0 (67.5) | 67 (64) ^a | 67 (64) ^a | 101.4 | | 101.4 | |
| | | | 101.7 | 102 ^f | | |
| 124.7 (124.7) | 127 ^b , 123 ⁱ | 127 ^b , 126 ^c | 126.8 | | 126.8 | |
| 133.1 (131.6) | 134 (131) ^a | 134 (131) ^a | 127.6 | 128 ^f | 127.5 | |
| | | | 199.0 | 200 ^f | 199.5 | |
| 148.2 | 151 ^a | 149 ^b , 148 ^c | * | 323 ^e | 324.6 | 323 ^e |
| 244 | 246 ^a | 246 ^{a,d} | 362 ^g | | 362 ^g | |
| 327.4 | 325 ^a | 332 ^{a,d} | 410.3 | 408 ^e | 410.3 | 408 ^e |
| * | 948 ^a | 948 ^a | * | 433 ^e | * | 433 ^e |
| | | | 717 ^g | 720 ^e | 718 ^g | 720 ^e |
| | | | 959.7 | | 959.2 | |

* Strong absorption due to HT-phonons in this frequency region

^a Low-temperature Raman data from Ref. [28]

^b Weak feature in the low-temperature spectra of Ref. [28]

^c Low-temperature Raman data from Ref. [29]

^d Fano resonance

^e Low-temperature Raman data from Ref. [19]

^f Weak feature in the low-temperature spectra of Ref. [19]

^g Low-temperature FIR data from Ref. [32]

^h Nonpolarized FIR transmittance data for a powdered sample from Ref. [26]

ⁱ Weak feature in the low-temperature (aa) spectrum of Ref. [29].

TABLE V. Comparison between the calculated vibrational frequencies of the Γ , Q, and Z-modes for the high-temperature $Pm\bar{m}n$ structure and measured frequencies for the HT- and LT-phases of α' - NaV_2O_5 . Corresponding irreducible representations for the $Fmm2$ LT-structure are indicated.

| $Pm\bar{m}n$ | calculated | measured | $Fmm2$ |
|--------------|------------------|----------|---------------|
| Γ | B_{3u} (TO-LO) | 955–957 | B_1 |
| | B_{1u} (TO-LO) | 961–1036 | A_1 |
| | B_{2g} | 962 | B_1 |
| | A_g | 964 | A_1 |
| Q | Q_1 | 969 | $2A_1 + 2A_2$ |
| | Q_2 | 973 | $2B_1 + 2B_2$ |
| Z | Z_5 | 985 | B_1 |
| | Z_6 | 1003 | B_1 |
| | Z_1 | 1018 | A_1 |
| | Z_5 | 1024 | A_1 |

* Strong absorption due to HT-phonons in this frequency region

^a Observed in unpolarized transmittance spectra of a powder sample

FIGURE CAPTIONS

FIG. 1. The structure of the low-temperature phase of α' - NaV_2O_5 . (a) Grey pyramids incorporate $\text{V}^{4.5+}$ ions. Black (white) pyramids are bigger (smaller) in size and are occupied by the V^{4+} (V^{5+}) ions. Balls represent Na atoms. (b) The ab -projection of the one V–O layer. Black (white) circles stand for V^{4+} (V^{5+}), while the grey ones represent $\text{V}^{4.5+}$. Arrows indicate the direction of displacements at the phase transition into the LT-phase.

FIG. 2. Transmittance spectra of α' - NaV_2O_5 at $T \approx 40 \text{ K} > T_c$ (dashed line) and $T = 8 \text{ K} < T_c$ (solid line) in $\mathbf{E} \parallel \mathbf{a}$, $\mathbf{E} \parallel \mathbf{b}$, and $\mathbf{E} \parallel \mathbf{c}$ polarizations of the incident light with $\mathbf{k} \parallel \mathbf{c}$ (a,b) and $\mathbf{k} \parallel \mathbf{a}$ (c). The sample thicknesses were $14 \mu\text{m}$ (a,b) and $150 \mu\text{m}$ (c). Arrows show new low-temperature modes below T_c .

FIG. 3. Absorbance difference spectra in $\mathbf{E} \parallel \mathbf{a}$ polarization for different temperatures showing the growth of new spectral lines below T_c . Spectra are vertically shifted for the sake of clarity.

FIG. 4. Absorbance difference spectra in $\mathbf{E} \parallel \mathbf{b}$ polarization: transition-induced modes with frequencies below 230 cm^{-1} .

FIG. 5. Absorbance difference spectra in $\mathbf{E} \parallel \mathbf{c}$ polarization. An asterisk marks weak features due to a leakage of $\mathbf{E} \parallel \mathbf{a}$ polarization. A weak intrinsic c -polarized mode near 133 cm^{-1} is shown by an arrow.

FIG. 6. Temperature dependences of the normalized shifts and linewidths of transition-induced modes. The insets show temperature dependences for the two modes from the high-temperature phase of α' - NaV_2O_5 .

FIG. 7. Peak position of selected transition-induced modes at different temperatures.

FIG. 8. Temperature dependence of the normalized oscillator strengths $f_T/f_{8\text{K}}$ for several transition-induced modes of α' - NaV_2O_5 . Lines are guides for the eye. Intensities of the X-ray reflections from Ref. [10] are shown by grey symbols. Asterisks represent the normalized integrated intensity of the spin-gap mode observed in optical ESR, as estimated from the data of Ref. [37].

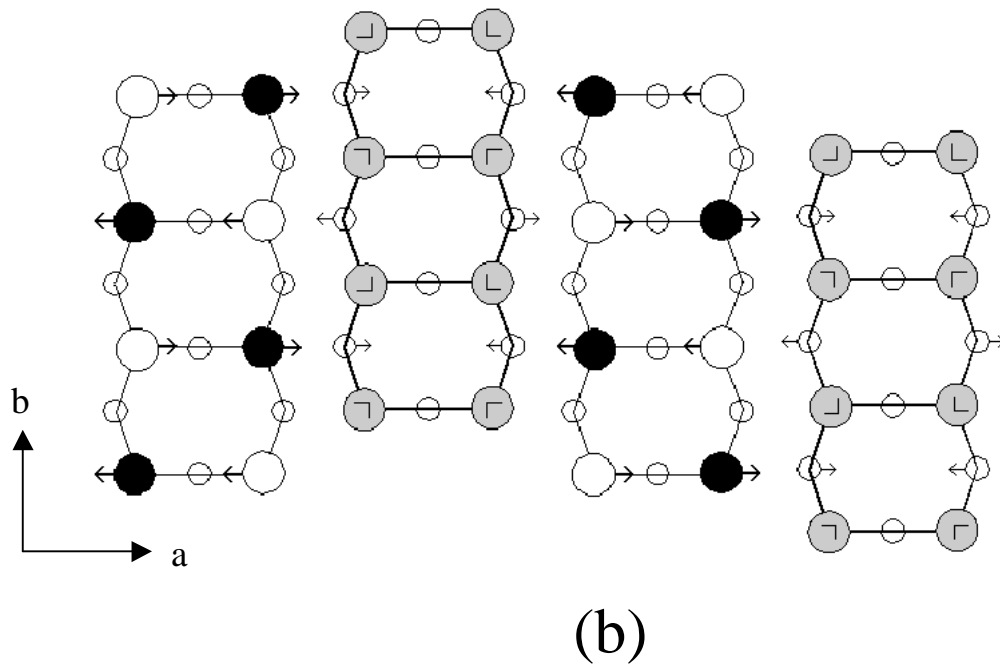
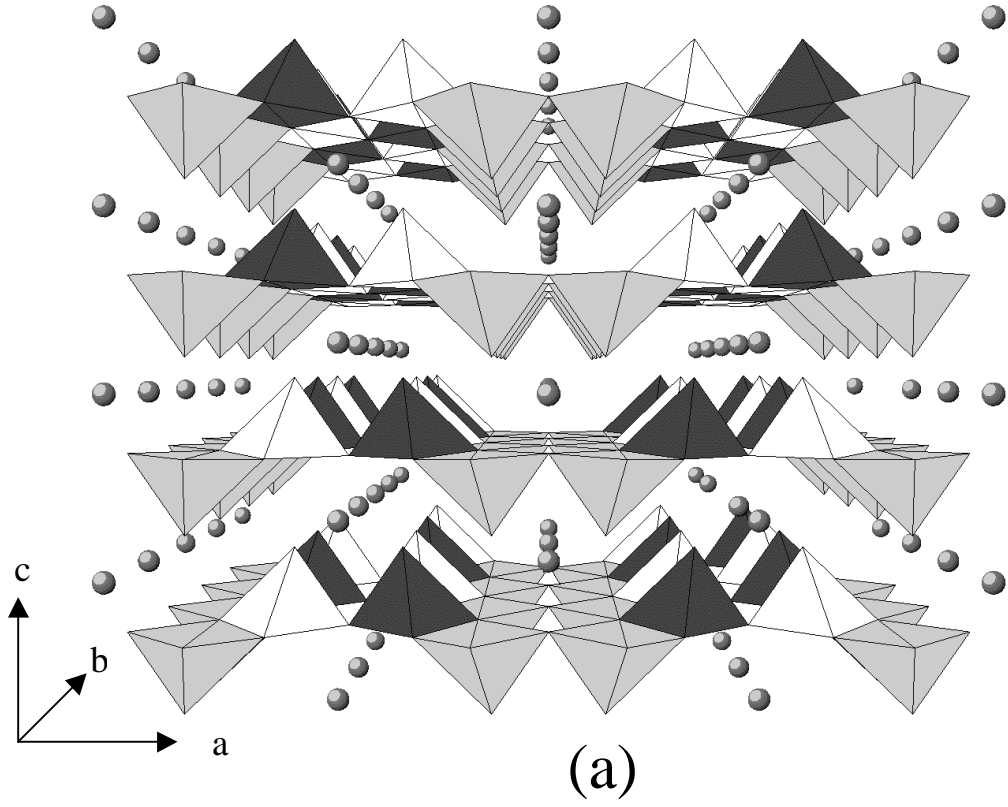
FIG. 9. Brillouin zone of the $Pmmn$ HT-structure of α' - NaV_2O_5 .

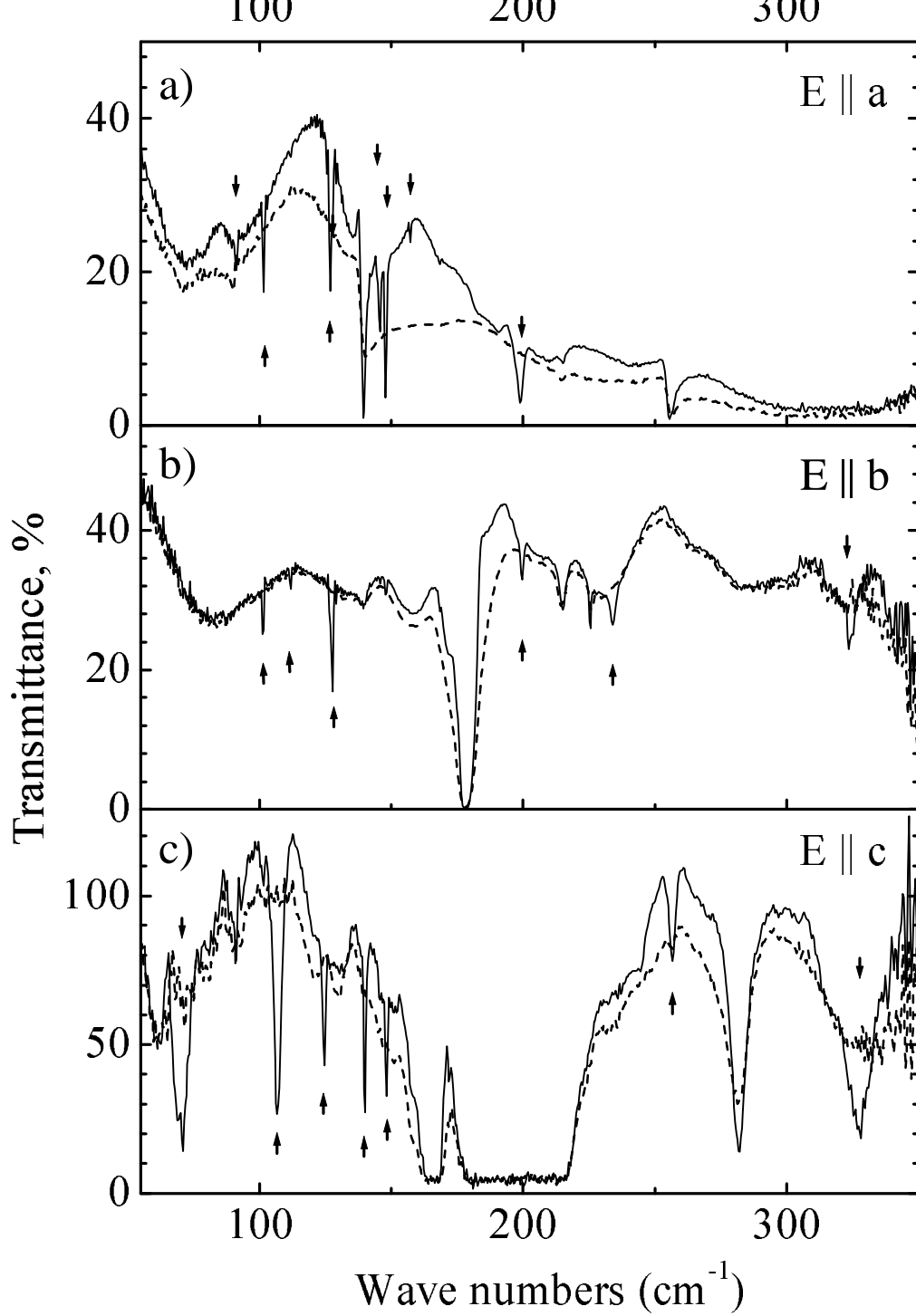
FIG. 10. Calculated phonon dispersion for the high-temperature $Pmmn$ structure of α' - NaV_2O_5 .

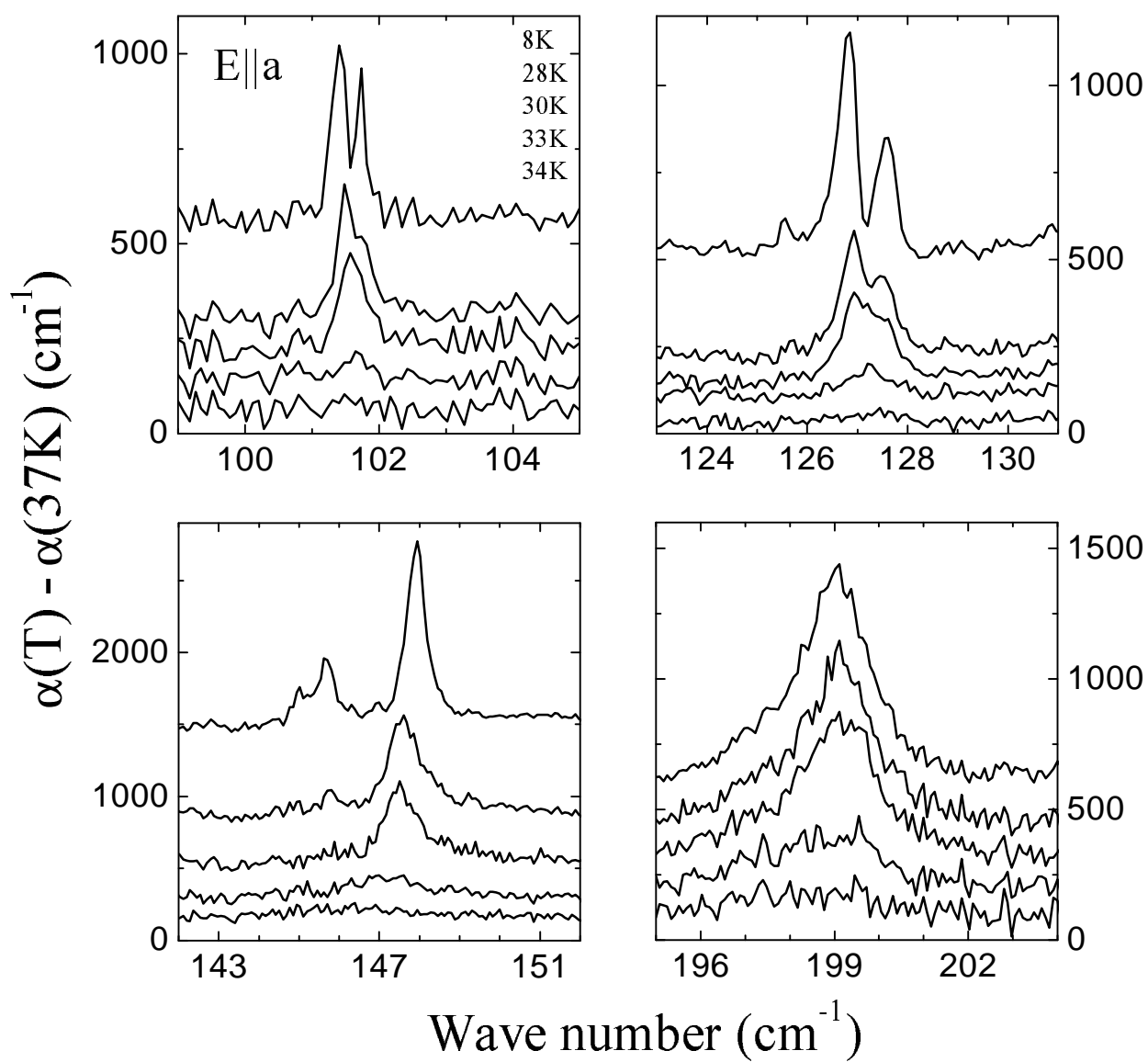
FIG. 11. Lowest-frequency transition-induced mode near 70 cm^{-1} in $\mathbf{E} \parallel \mathbf{c}$ transmittance spectrum of the $150 \mu\text{m}$ thick sample, corrected for the additional absorption of the epoxy layer (open circles). The dashed line was calculated using Eqs. (2)–(5) and one-oscillator approximation ($\omega = 70.0 \text{ cm}^{-1}$, $\gamma = 4.5 \text{ cm}^{-1}$, $f = 3.3 \cdot 10^{-3}$). The solid line represents the fit result for the two oscillators ($\omega_1 = 68.75 \text{ cm}^{-1}$, $\omega_2 = 70.9 \text{ cm}^{-1}$; $\gamma_1 = 2.2 \text{ cm}^{-1}$, $\gamma_2 = 3.2 \text{ cm}^{-1}$; $f_1 = 1.2 \cdot 10^{-3}$, $f_2 = 1.85 \cdot 10^{-3}$).

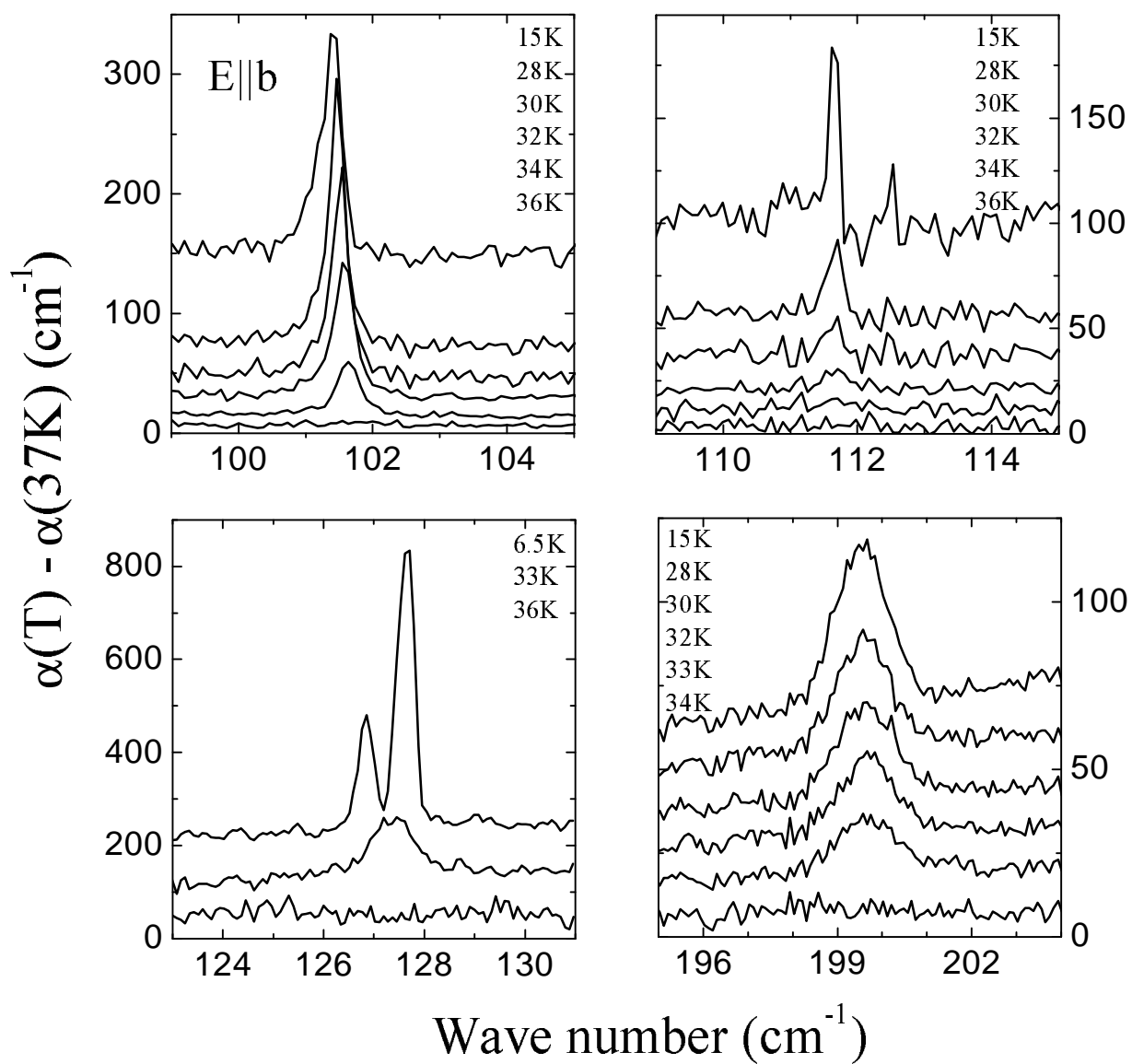
FIG. 12. Comparison between temperature dependences of normalized energies (frequencies) $\hbar\omega_T/\hbar\omega_{8\text{K}}$ of the transition-induced modes near 70 and 107 cm^{-1} and normalized magnetic gap $\Delta_T/\Delta_{7\text{K}}$ from inelastic neutron scattering measurements [10] (black circles).

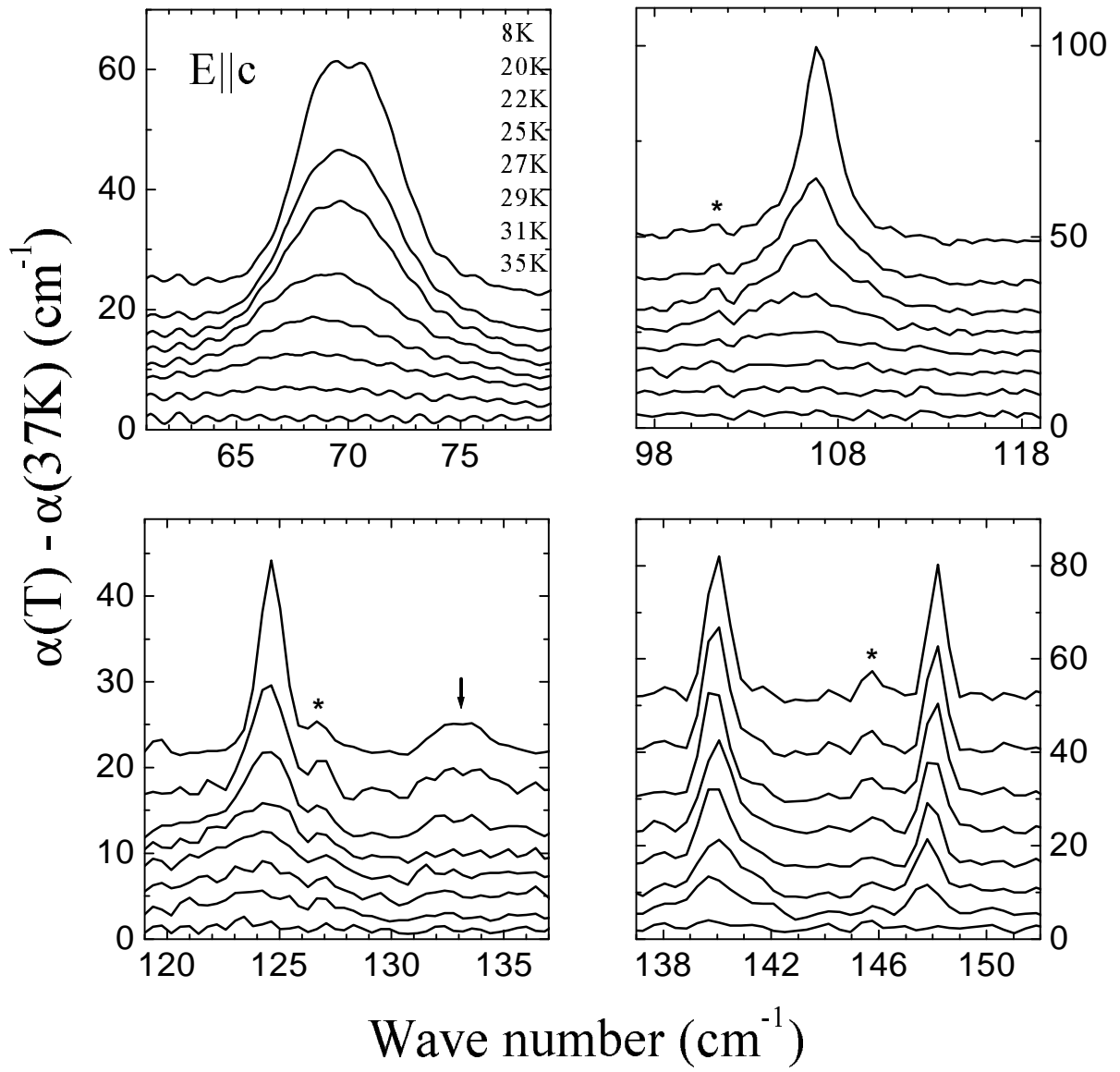
FIG. 13. Picture of atomic displacements of vanadium atoms for the lowest-frequency A_1 mode ($Fmm2$) folded from the Q -point of ($Pm\bar{m}n$) high-temperature structure. (a) one ab -layer. Only vanadium atoms are shown. Displacements along the positive (negative) direction of the c -axis are indicated by points (crosses). (b) Vanadium atoms 1 and 2 at the opposite ends of a ladder rung, together with oxygen at the middle of a rung and two apical oxygens. When V2 approaches apical oxygen, V1 goes moves away from it, which stimulates an asymmetric charge distribution along the rung.

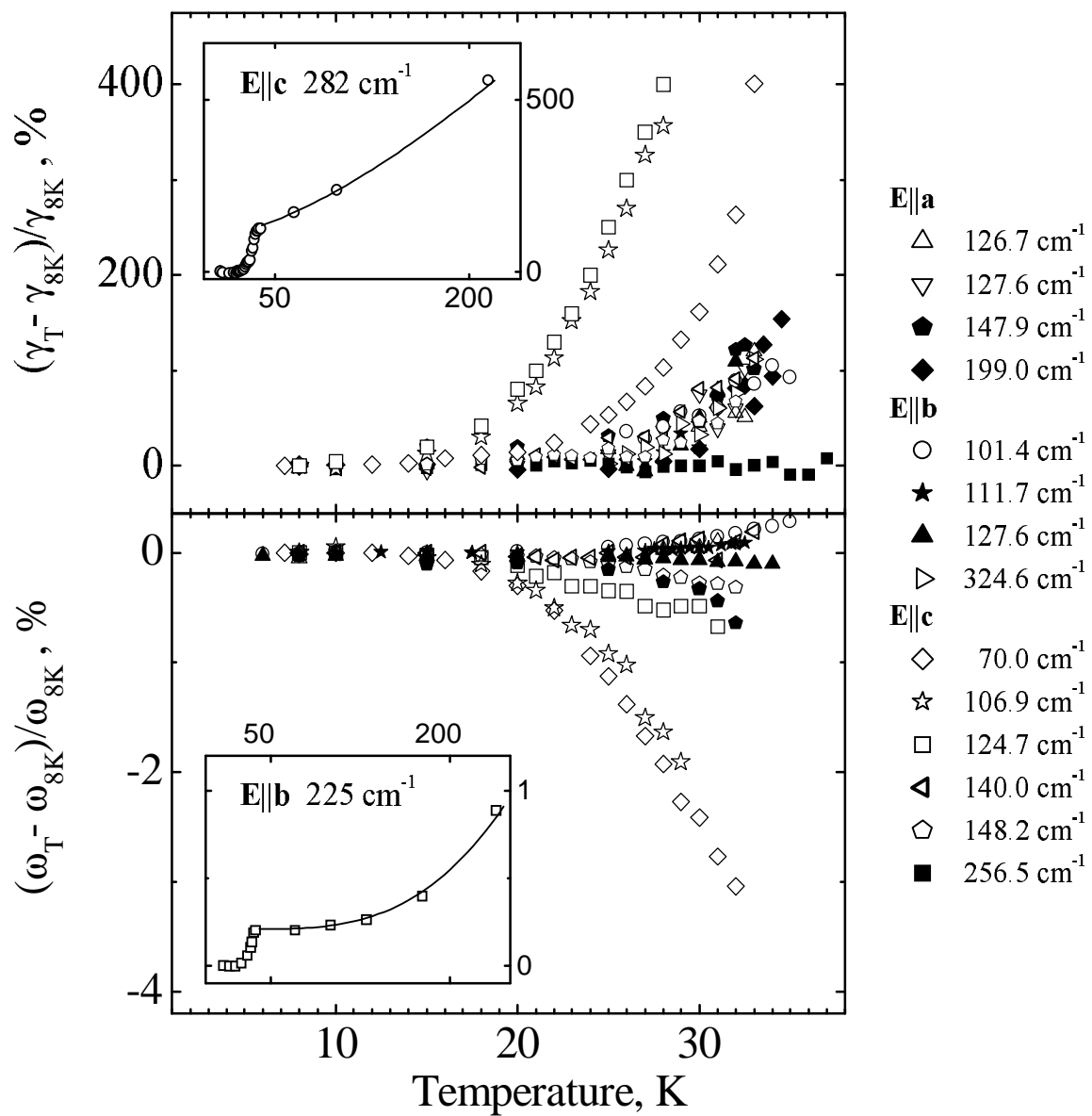


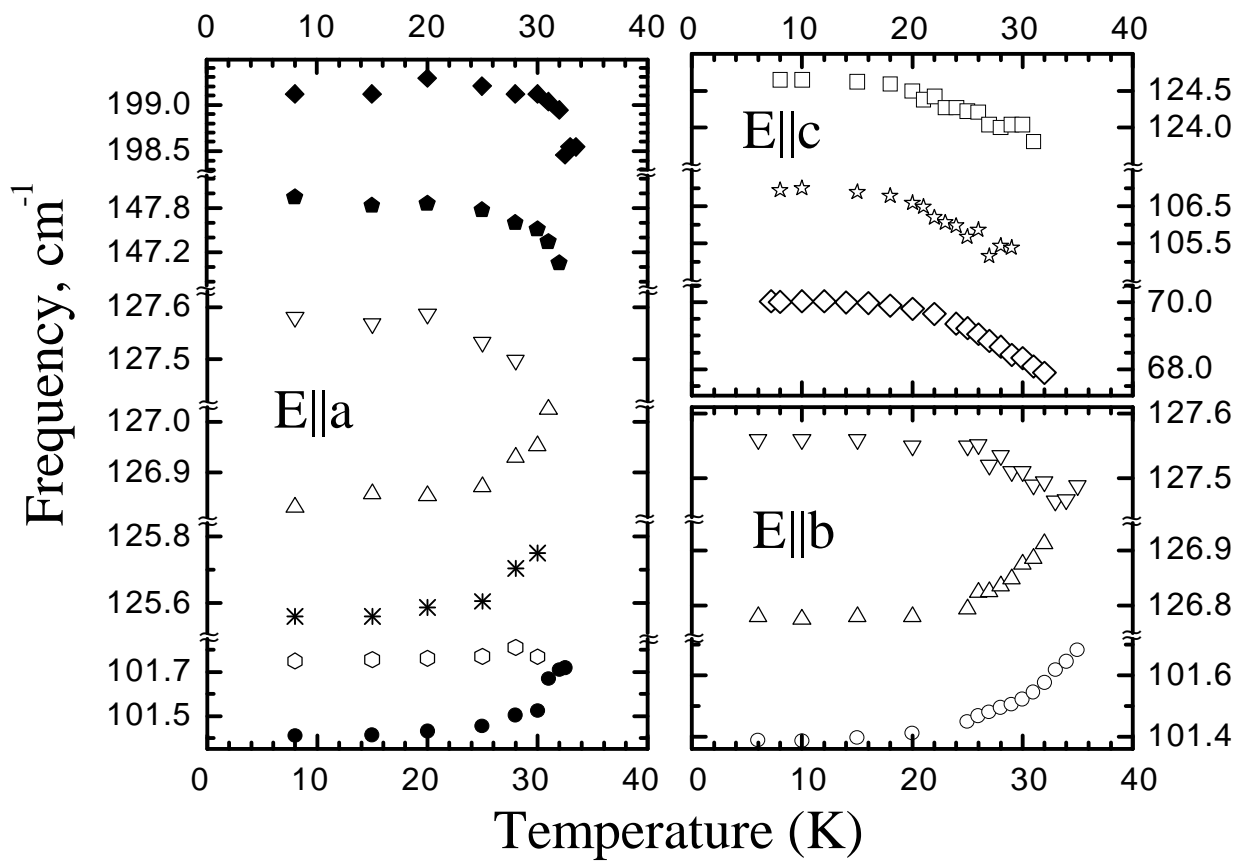


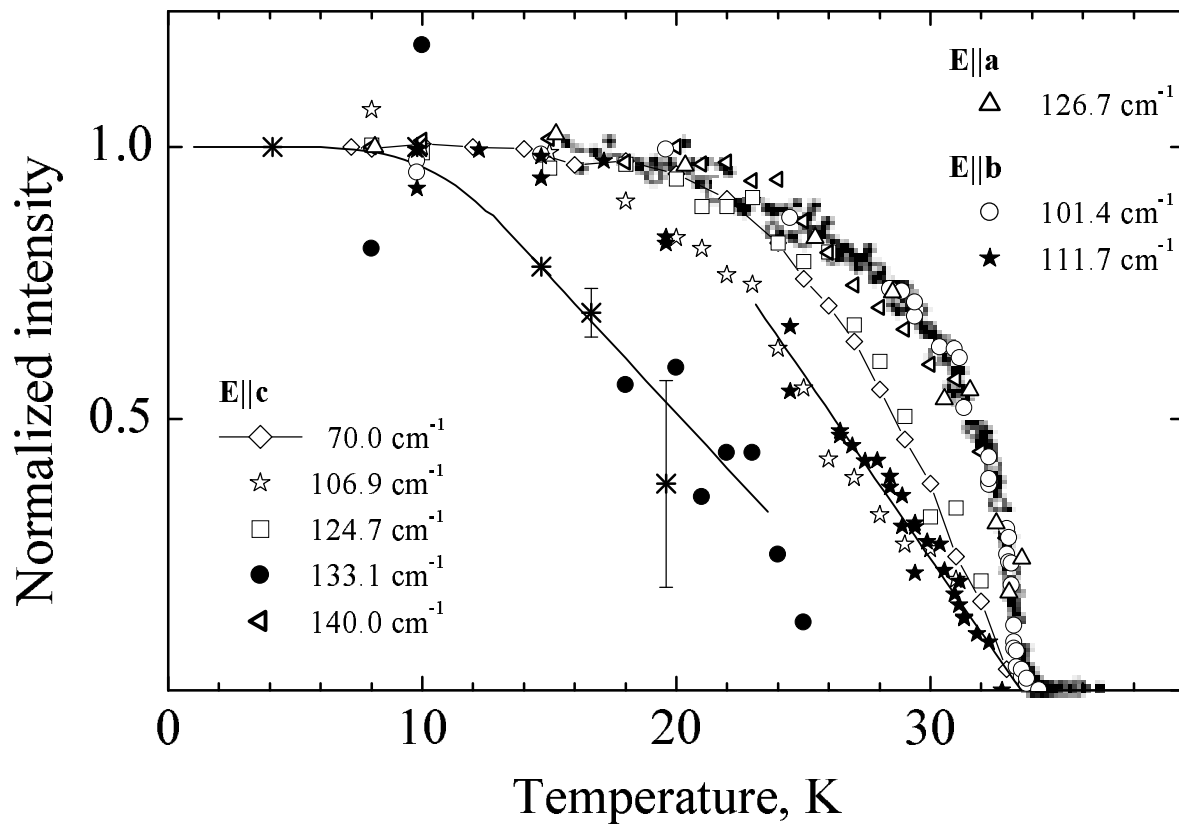


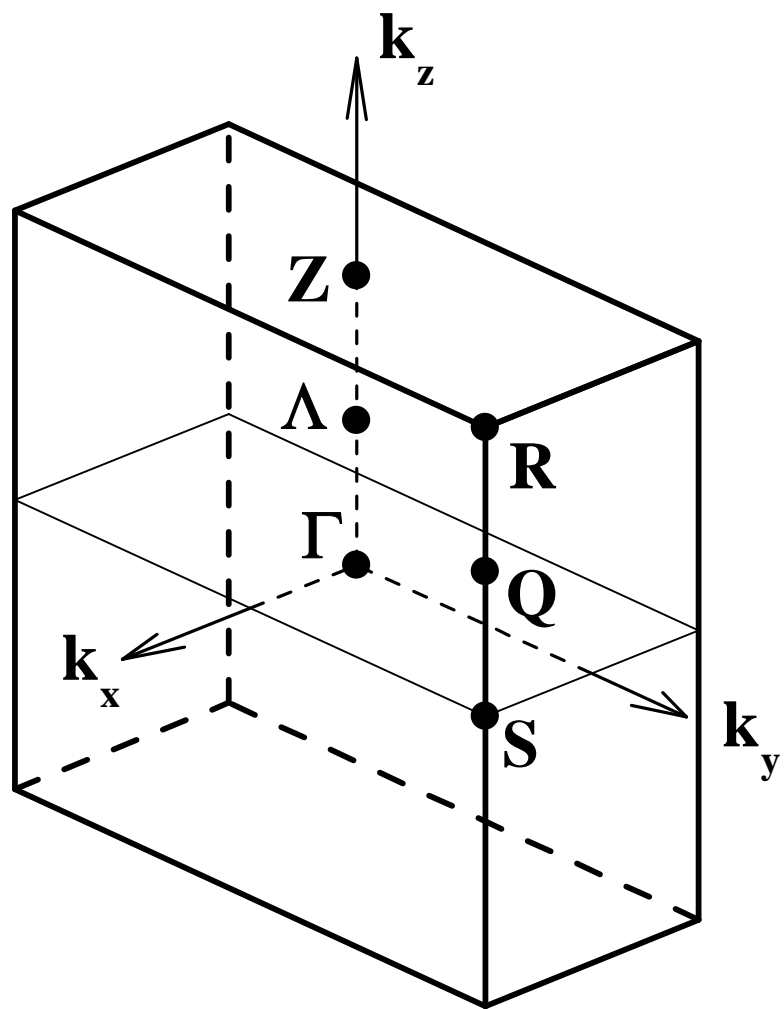


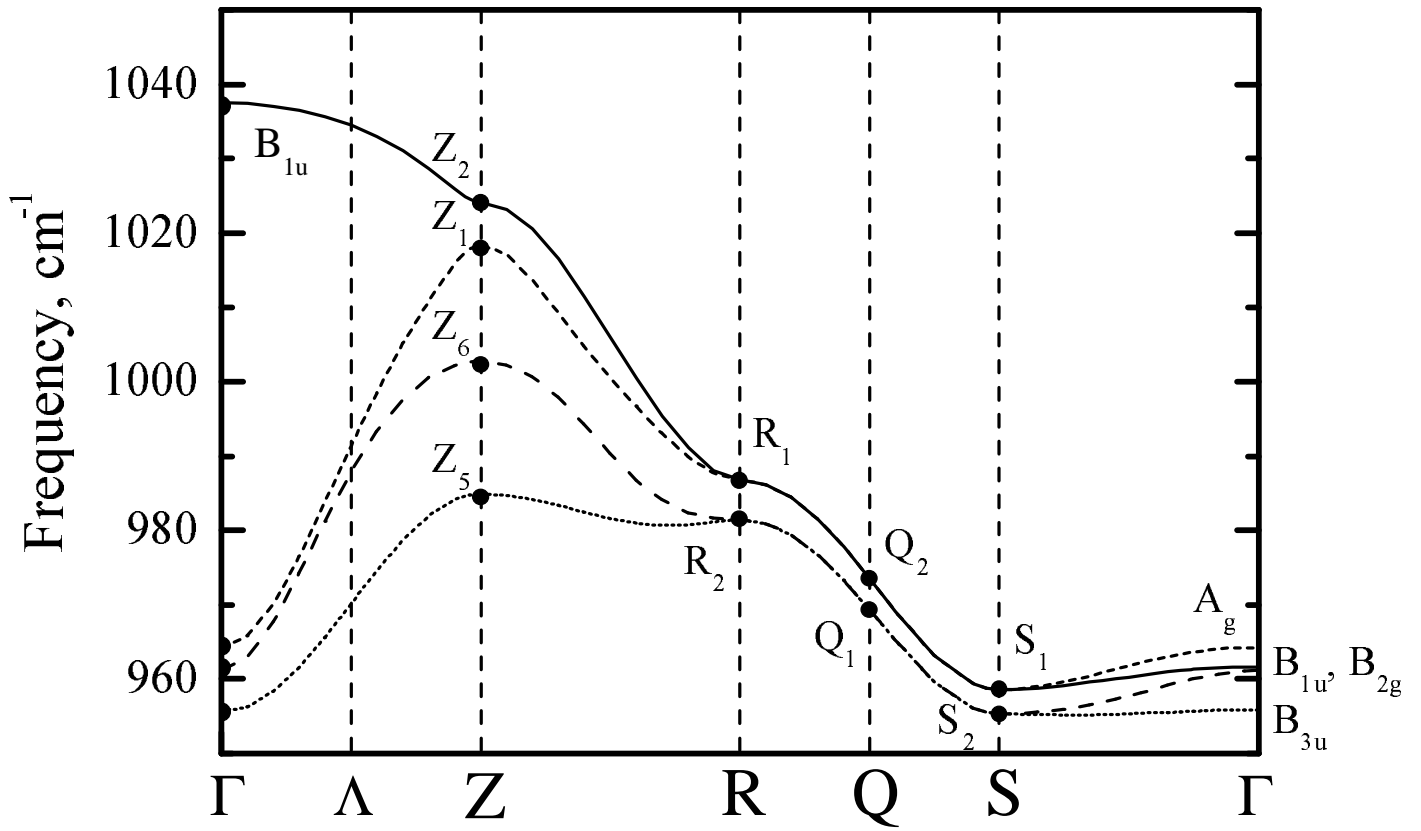


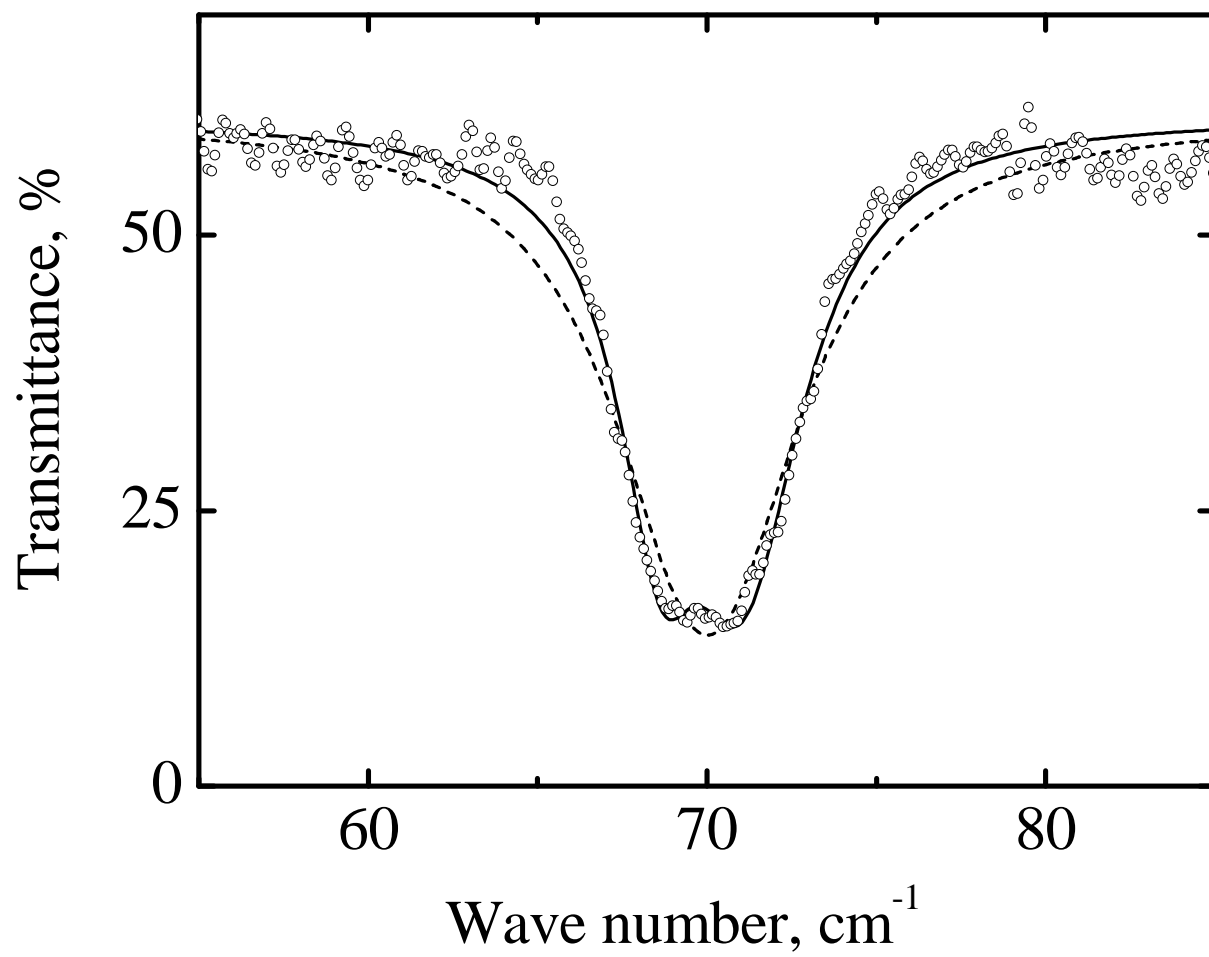


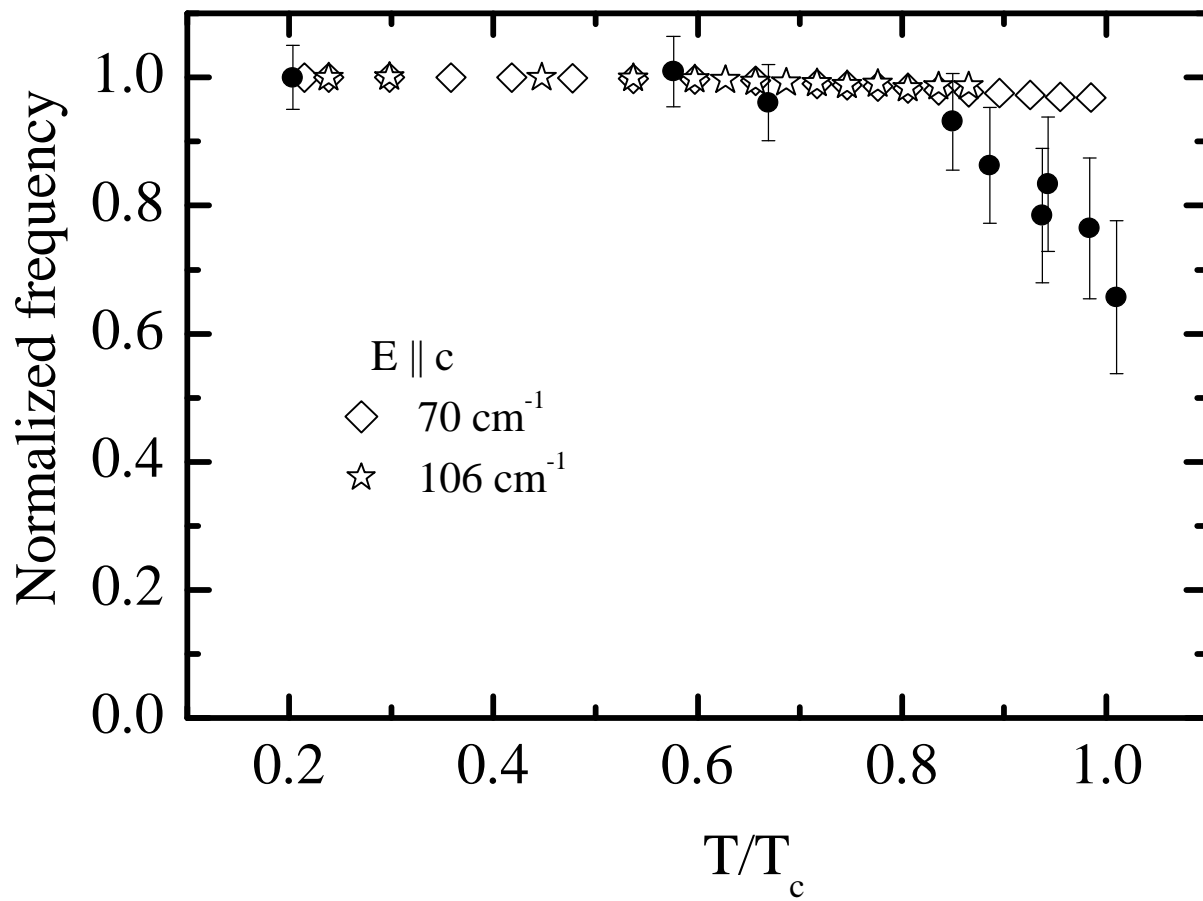


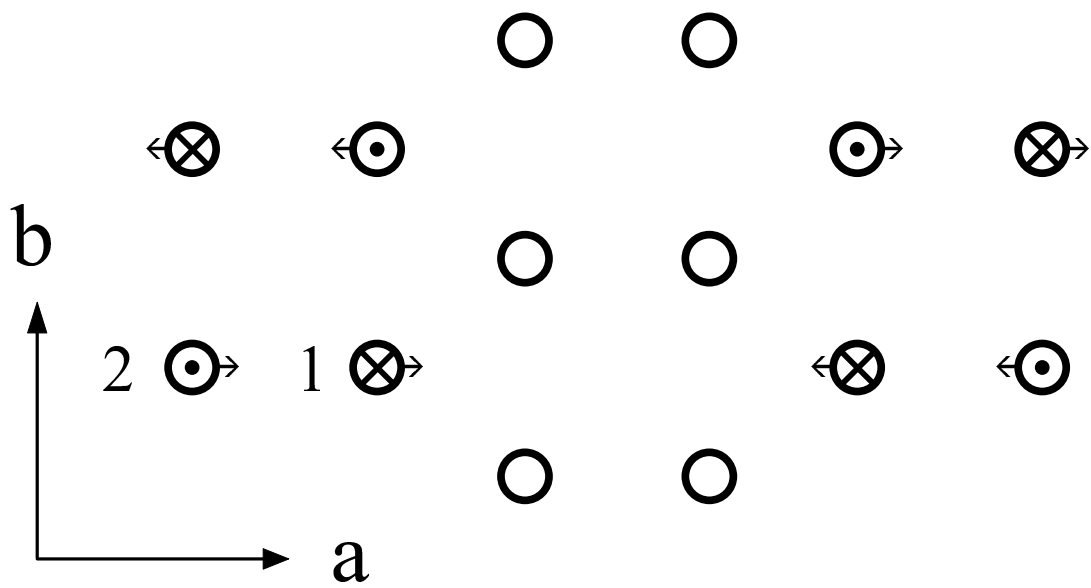




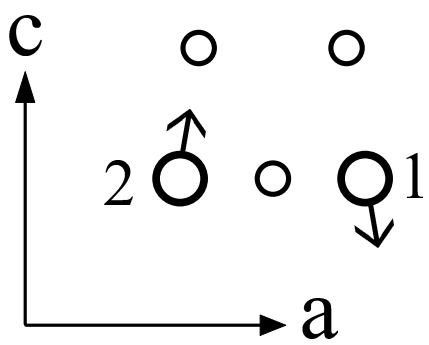








(a)



(b)